Supplementary Information

Redox-Based Defect Detection in Packed DNA: Insights from Hybrid Quantum Mechanical/Molecular Mechanics Molecular Dynamics Simulations

Murat Kılıç[†], Polydefkis Diamantis[†], Sophia K. Johnson, Oliver Toth, and Ursula Rothlisberger[*]

Laboratory of Computational Chemistry and Biochemistry, Institute of Chemical Sciences and Engineering, École Polytechnique Fédérale de Lausanne (EPFL), CH-1015 Lausanne, Switzerland

E-mail: ursula.roethlisberger@epfl.ch

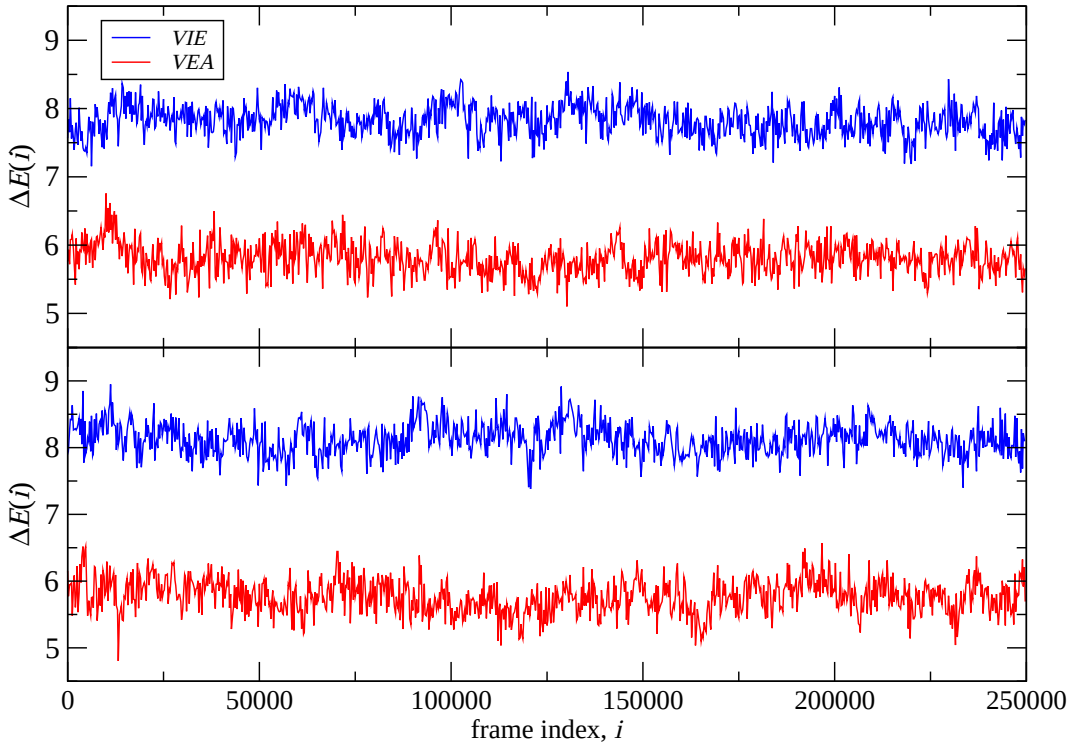

Figure 1: Time series of the vertical ionization energies (*VIE*s) and vertical electron affinities (*VEA*s) used for the determination of the vertical energy gap distributions and redox properties of the native G-rich **regions 1** (**top**) and **2** (**bottom**).

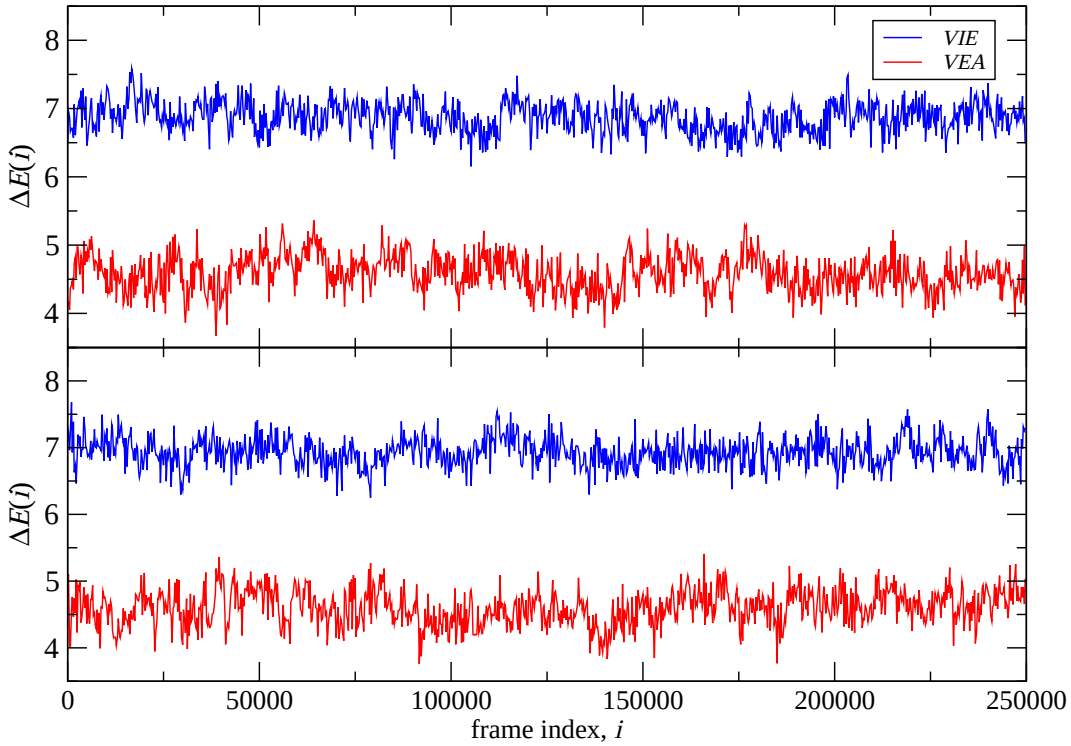

Figure 2: Time series of the *VIE*s and *VEA*s used for the determination of the vertical energy gap distributions and redox properties of the defect systems in which the 8-oxoguanine (8oxoG) base was placed in G-rich **regions 1** (**top**) and **2** (**bottom**).

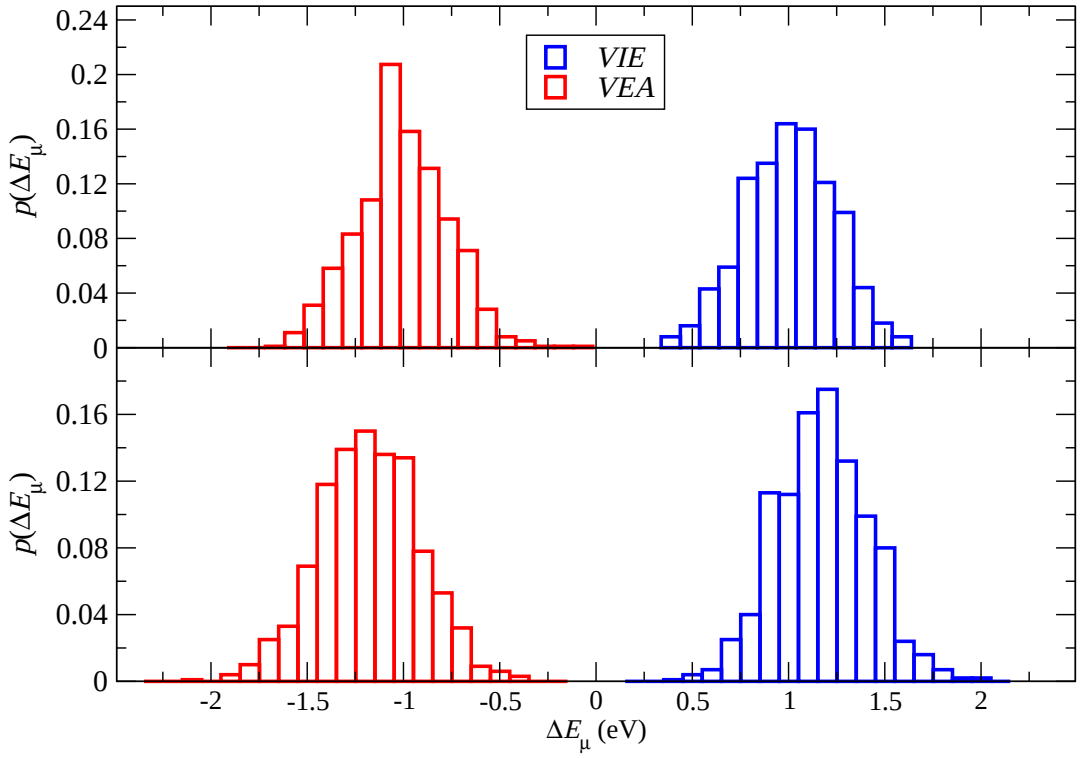

Figure 3: *VIE* and *VEA* distributions for the native G-rich **regions 1** (**top**) and **2** (**bottom**).

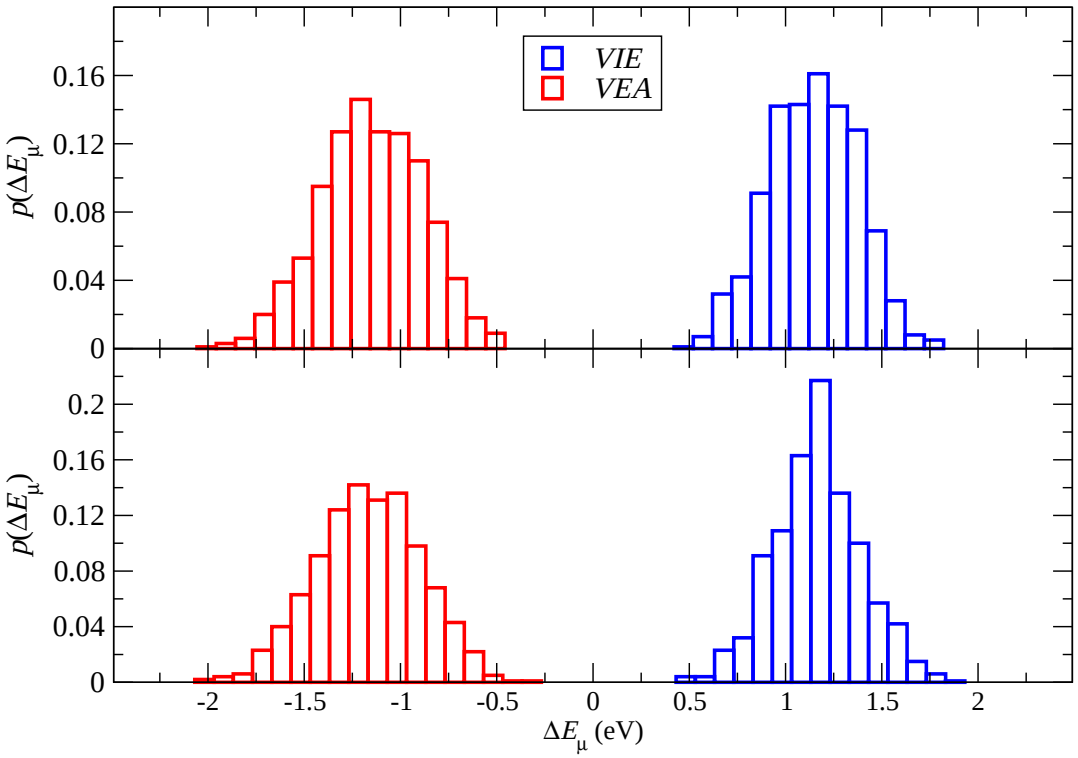

Figure 4: *VIE* and *VEA* distributions for the defect systems in which 8oxoG was placed in in G-rich **regions 1** (**top**) and **2** (**bottom**).

Table 1: G-rich **region 1** systems: Root mean square fluctuations (RMSFs) for the DNA residues belonging in the QM region of the native (left) and 8oxoG-containing (right) systems.

Native				8oxoG			
Reduced		Oxidized		Reduced		Oxidized	
ResID	RMSF (Å)	ResID	RMSF (Å)	ResID	RMSF (Å)	ResID	RMSF (Å)
58	0.46	58	0.47	58	0.43	58	0.44
59	0.44	59	0.40	59	0.46	59	0.39
60	0.43	60	0.40	60	0.48	60	0.41
233	0.58	233	0.45	233	0.47	233	0.43
234	0.55	234	0.40	234	0.50	234	0.61
235	0.51	235	0.61	235	0.63	235	0.54

Table 2: G-rich **region 2** systems: Root mean square fluctuations (RMSFs) for the DNA residues belonging in the QM region of the native (left) and 8oxoG-containing (right) systems.

Native				8oxoG			
Reduced		Oxidized		Reduced		Oxidized	
ResID	RMSF (Å)	ResID	RMSF (Å)	ResID	RMSF (Å)	ResID	RMSF (Å)
87	0.52	87	0.58	87	0.46	87	0.49
88	0.48	88	0.48	88	0.42	88	0.40
89	0.53	89	0.48	89	0.44	89	0.39
204	0.67	204	0.45	204	0.42	204	0.50
205	0.44	205	0.45	205	0.38	205	0.44
206	0.56	206	0.44	206	0.43	206	0.48

Table 3: G-rich **region 1** systems: QM-treated DNA and neighboring protein residues sharing a strong intermolecular interaction in the native (left) and 8oxoG-containing (right) systems.

Native				8oxoG			
Reduced		Oxidized		Reduced		Oxidized	
ResID_{DNA}	$\text{ResID}_{Pro.}$	ResID_{DNA}	$\text{ResID}_{Pro.}$	ResID_{DNA}	$\text{ResID}_{Pro.}$	ResID_{DNA}	$\text{ResID}_{Pro.}$
58	–	58	–	58	–	58	–
59	–	59	–	59	–	59	318
60	407	60	401 / 407	60	318 / 401	60	318 / 407
233	–	233	–	233	–	233	–
234	–	234	–	234	–	234	–
235	391	235	–	235	–	235	–

Table 4: G-rich **region 2** systems: QM-treated DNA and neighboring protein residues sharing an intermolecular interaction in the native (left) and 8oxoG-containing (right) systems. With the exception of a strong (206-731) and a weak (204-688) interaction found for for the oxidized native system, no intermolecular interactions were identified.

Native				8oxoG			
Reduced		Oxidized		Reduced		Oxidized	
ResID_{DNA}	$\text{ResID}_{Pro.}$	ResID_{DNA}	$\text{ResID}_{Pro.}$	ResID_{DNA}	$\text{ResID}_{Pro.}$	ResID_{DNA}	$\text{ResID}_{Pro.}$
87	–	87	–	87	–	87	–
88	–	88	–	88	–	88	–
89	–	89	–	89	–	89	–
204	–	204	688	204	–	204	–
205	–	205	–	205	–	205	–
206	–	206	731	206	–	206	–

Table 5: The 3 DNA base pairs which comprise the G-rich **region 2** systems have a greater number of average H-bonding interactions with solvent molecules throughout the classical molecular dynamics simulation than the 3 DNA base pairs of the G-rich **region 1** systems indicating that **region 2** is more solvent-exposed than **region 1** regardless of the presence or absence of the 8oxoguanine defect. Average H-bonding interactions between the DNA bases and solvent molecules were calculated with GROMACS hydrogen bonding tool with counts viable hydrogen bonding interactions throughout a trajectory for selected donor and acceptor groups.

Native		8oxoG	
Region 1	Region 2	Region 1	Region 2
46.70	53.65	50.87	54.38

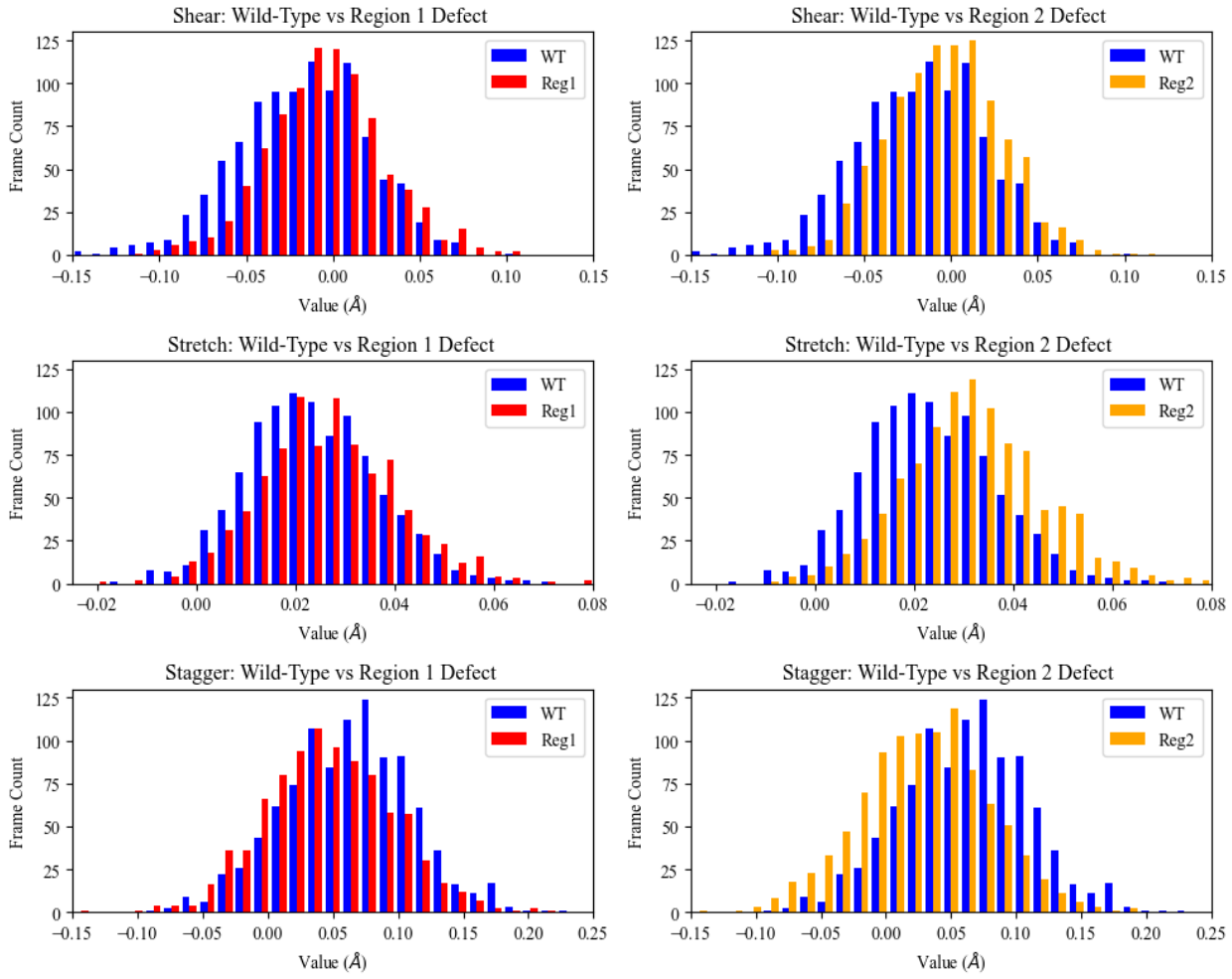

Figure 5: Population distributions of intrabase translational parameters (shear, stretch, and stagger) for wild-type system (WT, blue) vs region 1 defect system (Reg1, red) and for wild-type system (WT, blue) vs region 2 defect system (Reg2, orange). The systems do not include in their analysis the 40 base pairs associated with tail regions.

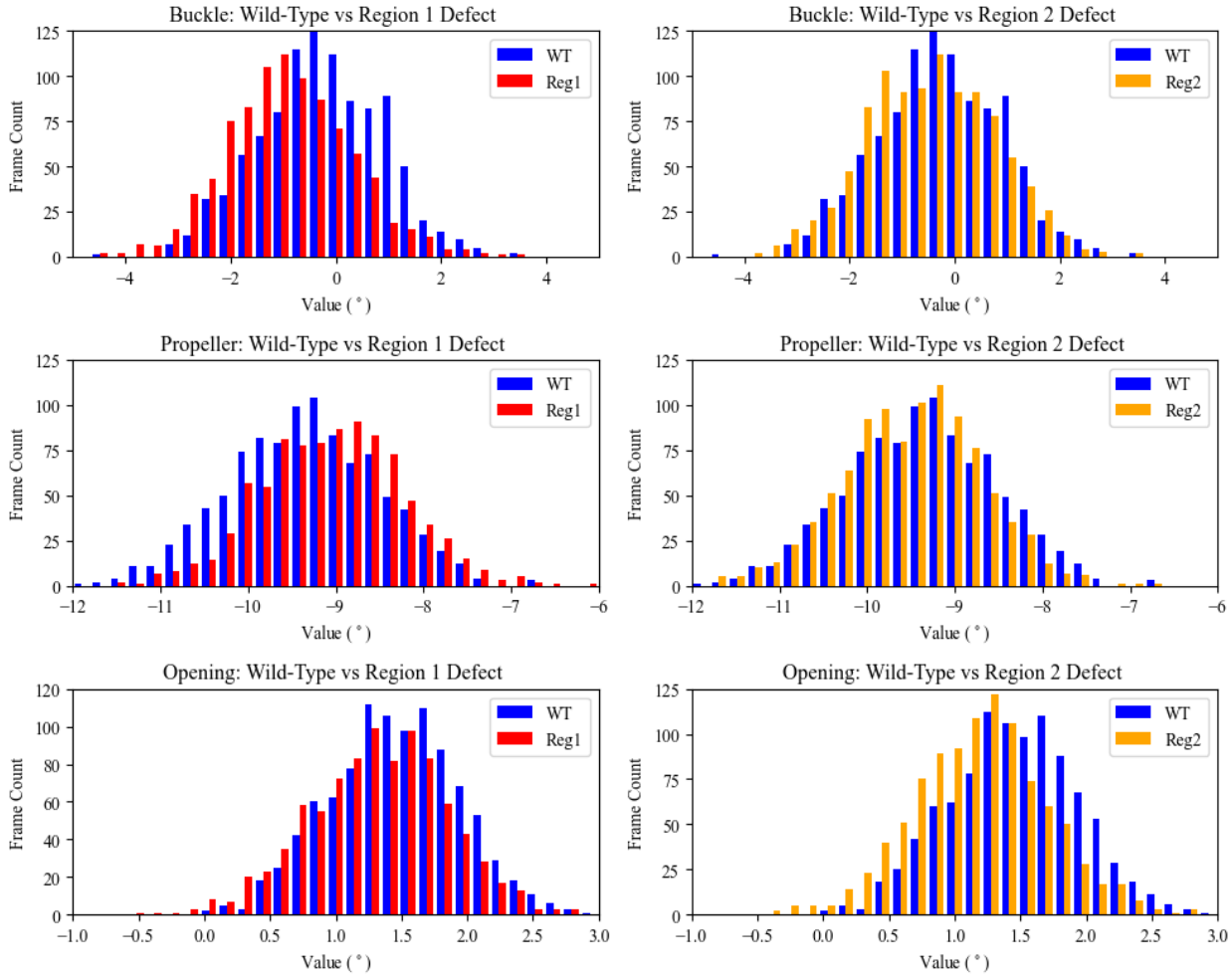

Figure 6: Population distributions of intrabase rotational parameters (buckle, propeller, and opening) for wild-type system (WT, blue) vs region 1 defect system (Reg1, red) and for wild-type (WT, blue) vs region 2 defect system (Reg2, orange). The systems do not include in their analysis the 40 base pairs associated with tail regions.

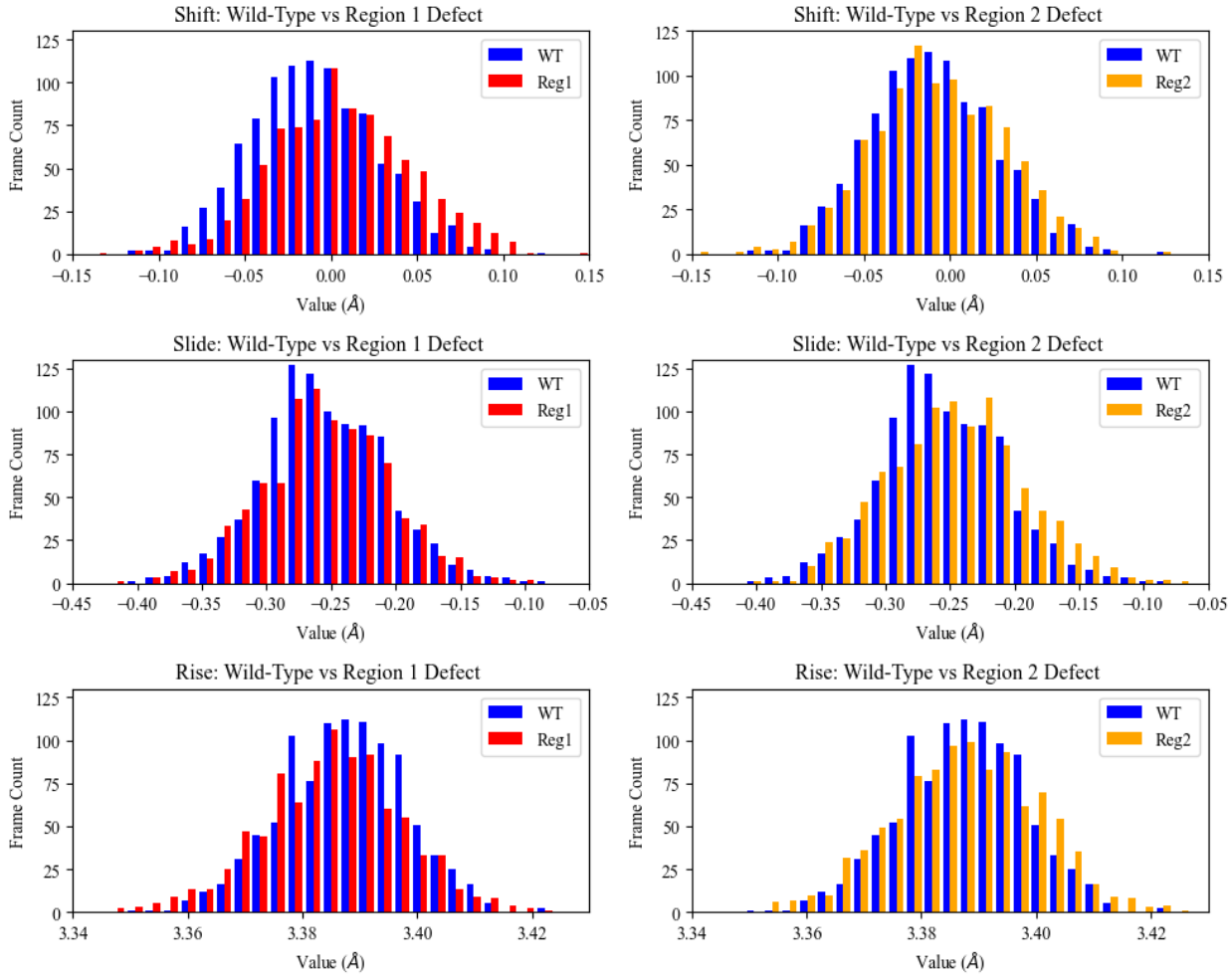

Figure 7: Population distributions of interbase translational parameters (shift, slide, and rise) for wild-type system (WT, blue) vs region 1 defect system (Reg1, red) and for wild-type system (WT, blue) vs region 2 defect system (Reg2, orange). The systems do not include in their analysis the 40 base pairs associated with tail regions.

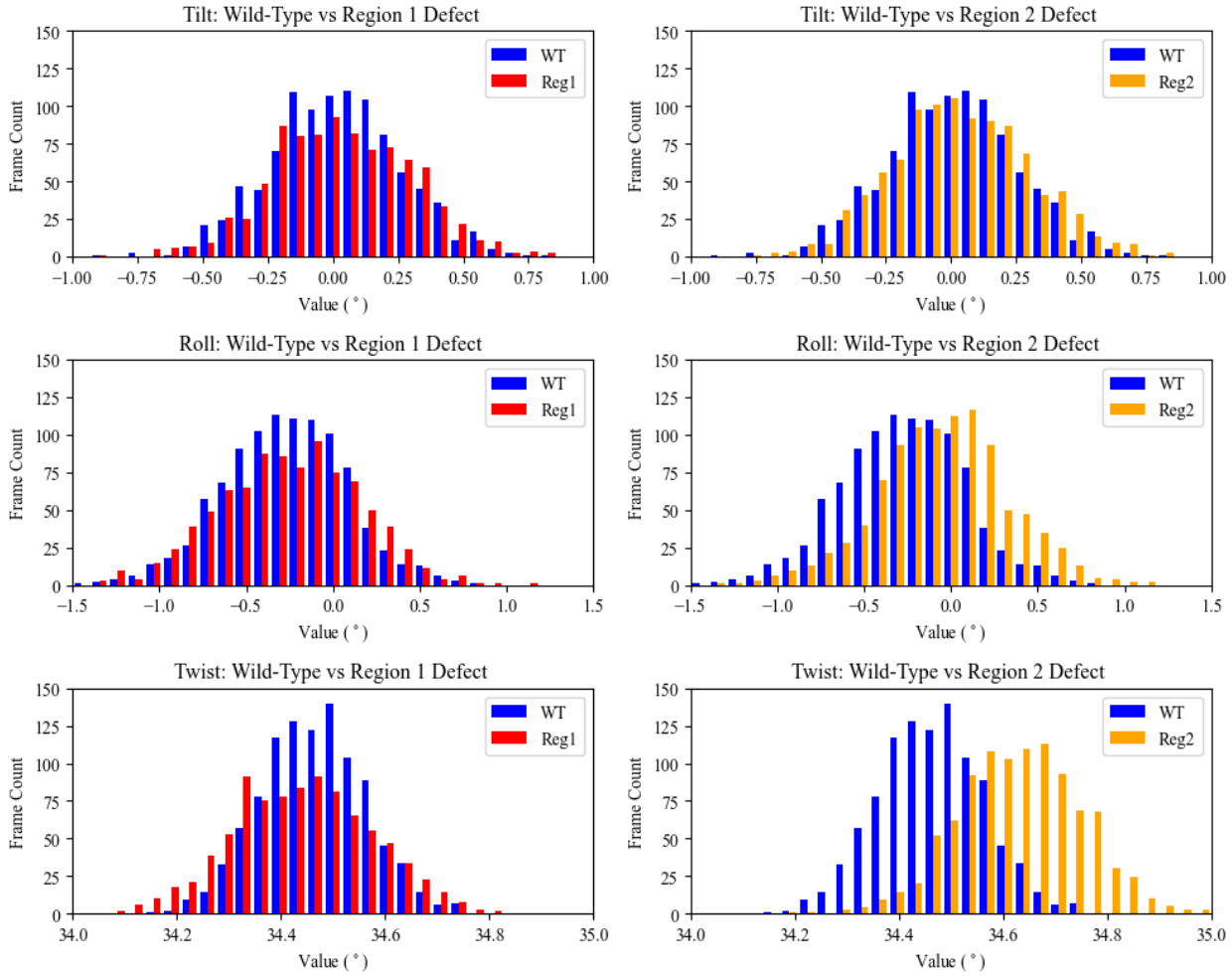

Figure 8: Population distributions of interbase rotational parameters: tilt, roll, and twist for wild-type system (WT, blue) vs region 1 defect system (Reg1, red) and for wild-type system (WT, blue) vs region 2 defect system (Reg2, orange). The systems do not include in their analysis the 40 base pairs associated with tail regions.

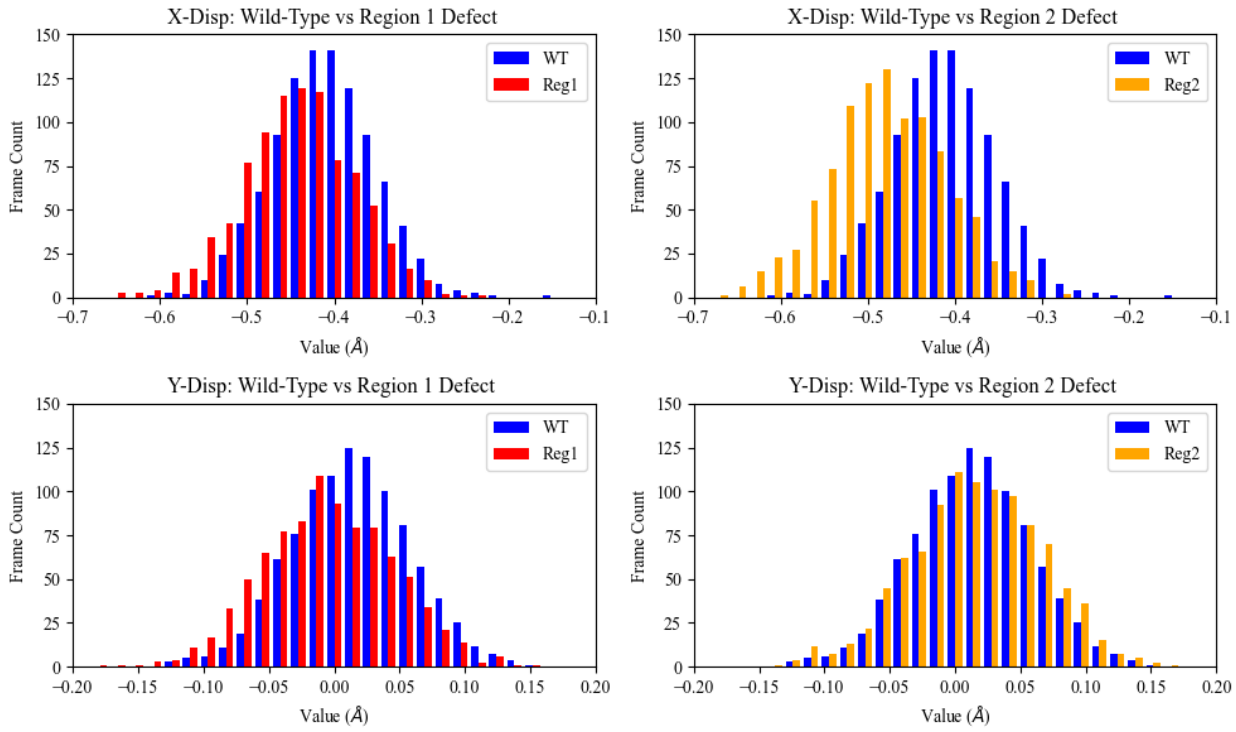

Figure 9: Population distributions of base-axis translational parameters (X- and Y-displacement) for wild-type system (WT, blue) vs region 1 defect system (Reg1, red) and for wild-type system (WT, blue) vs region 2 defect system (Reg2, orange). The systems do not include in their analysis the 40 base pairs associated with tail regions.

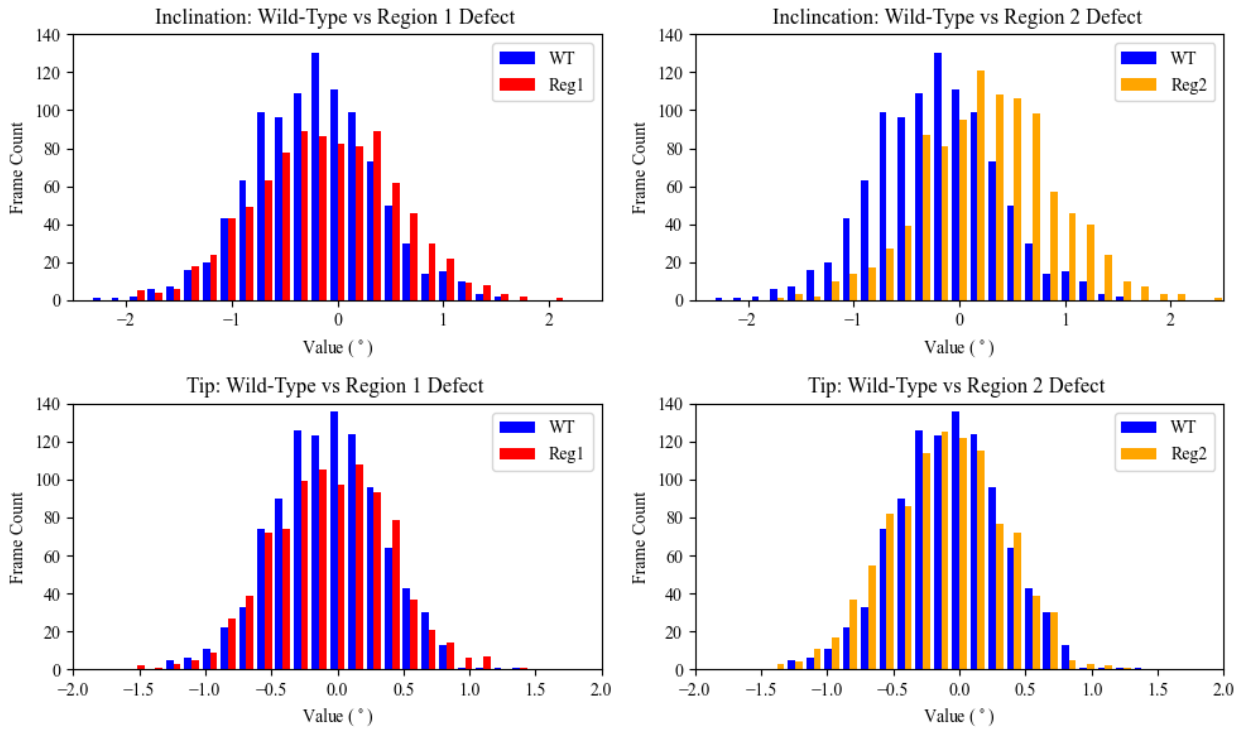

Figure 10: Population distributions of the base-axis rotational parameters (inclination and tip) for wild-type system (WT, blue) vs region 1 defect system (Reg1, red) and for wild-type system (WT, blue) vs region 2 defect system (Reg2, orange). The systems do not include in their analysis the 40 base pairs associated with tail regions.

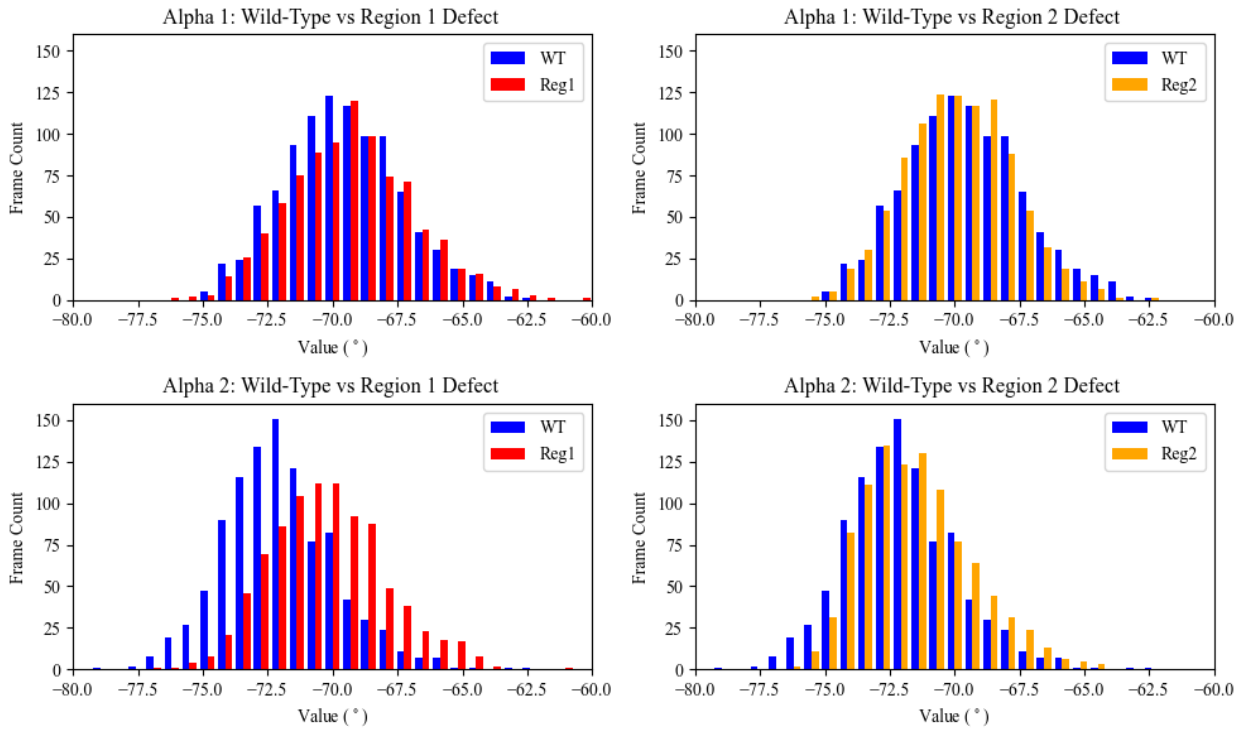

Figure 11: Population distributions of the alpha torsional angle of both DNA strands 1 and 2 for wild-type system (WT, blue) vs region 1 defect system (Reg1, red) and for wild-type system (WT, blue) vs region 2 defect system (Reg2, orange). The systems do not include in their analysis the 40 base pairs associated with tail regions.

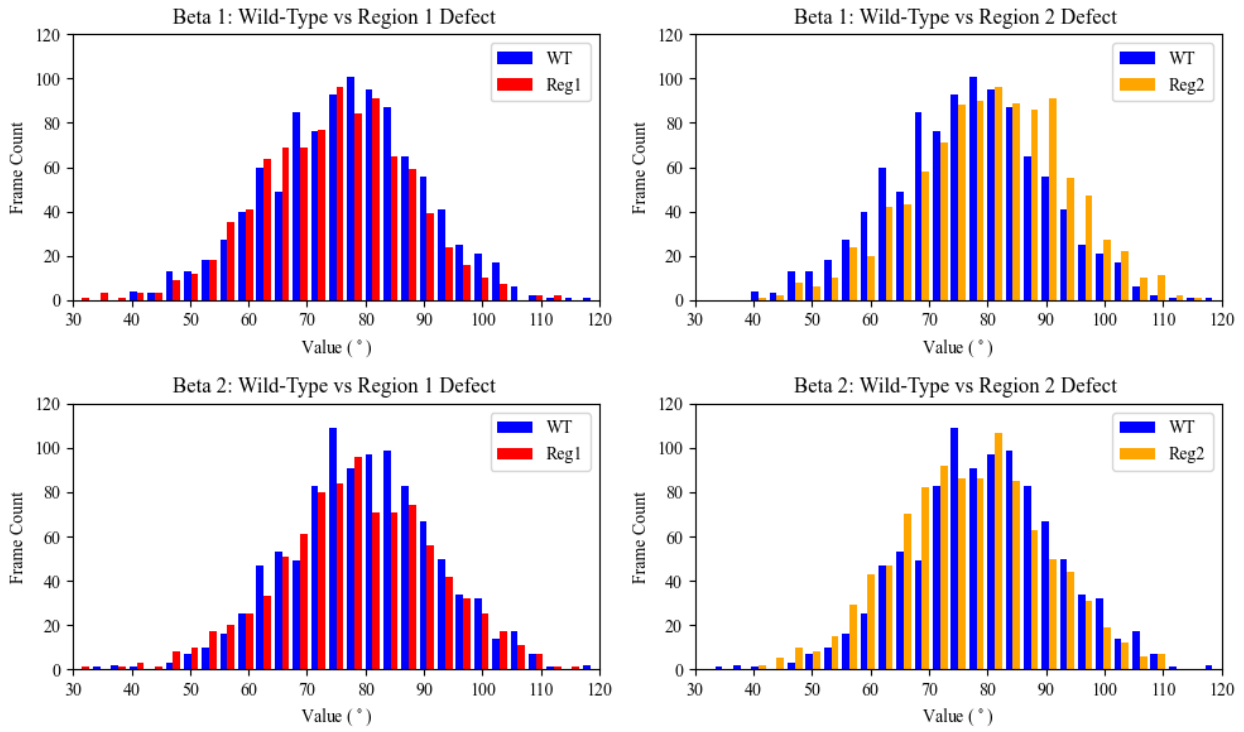

Figure 12: Population distributions of the beta torsional angle of both DNA strands 1 and 2 for wild-type system (WT, blue) vs region 1 defect system (Reg1, red) and for wild-type system (WT, blue) vs region 2 defect system (Reg2, orange). The systems do not include in their analysis the 40 base pairs associated with tail regions.

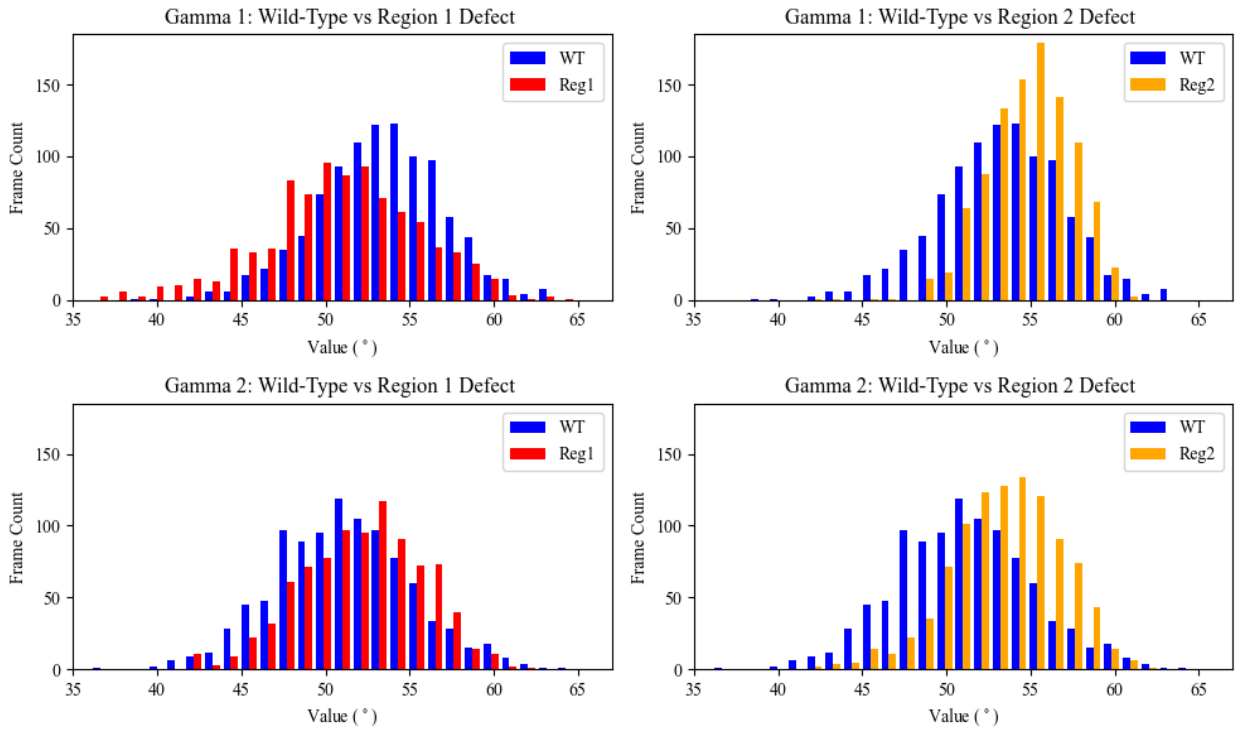

Figure 13: Population distributions of the gamma torsional angle of both DNA strands 1 and 2 for wild-type system (WT, blue) vs region 1 defect system (Reg1, red) and for wild-type system (WT, blue) vs region 2 defect system (Reg2, orange). The systems do not include in their analysis the 40 base pairs associated with tail regions.

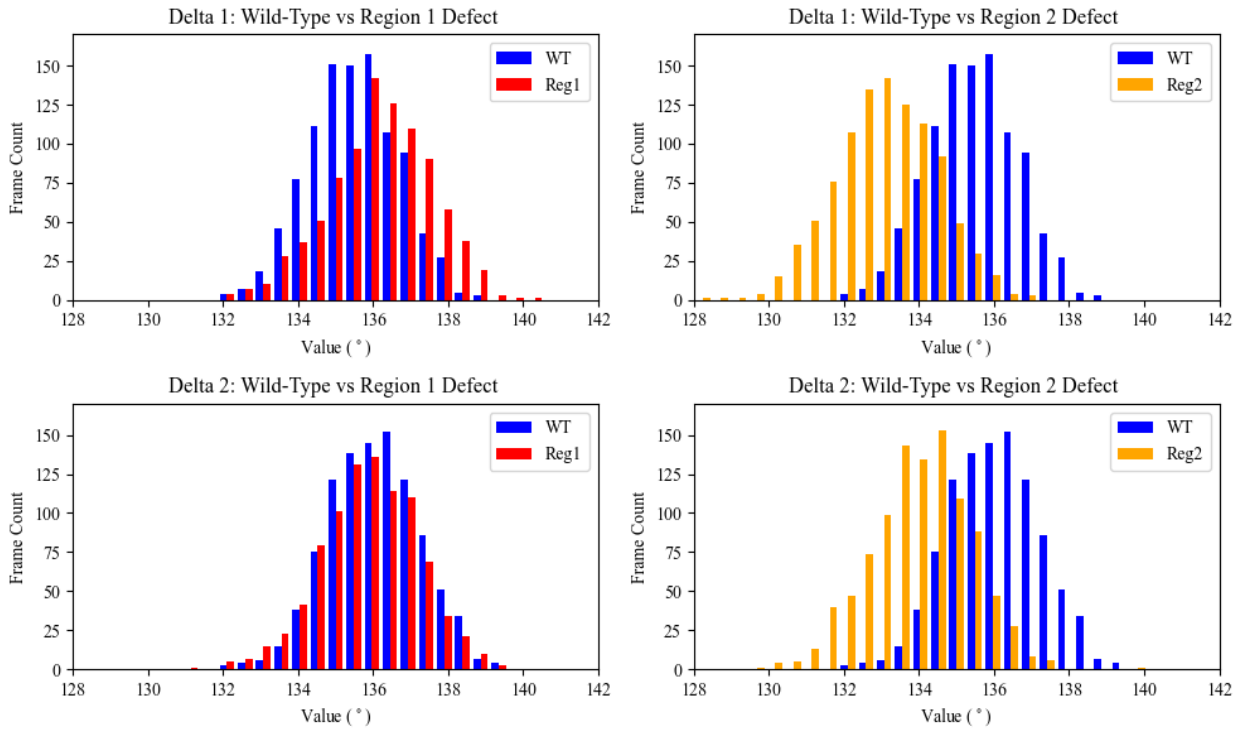

Figure 14: Population distributions of the delta torsional angle of both DNA strands 1 and 2 for wild-type system (WT, blue) vs region 1 defect system (Reg1, red) and for wild-type system (WT, blue) vs region 2 defect system (Reg2, orange). The systems do not include in their analysis the 40 base pairs associated with tail regions.

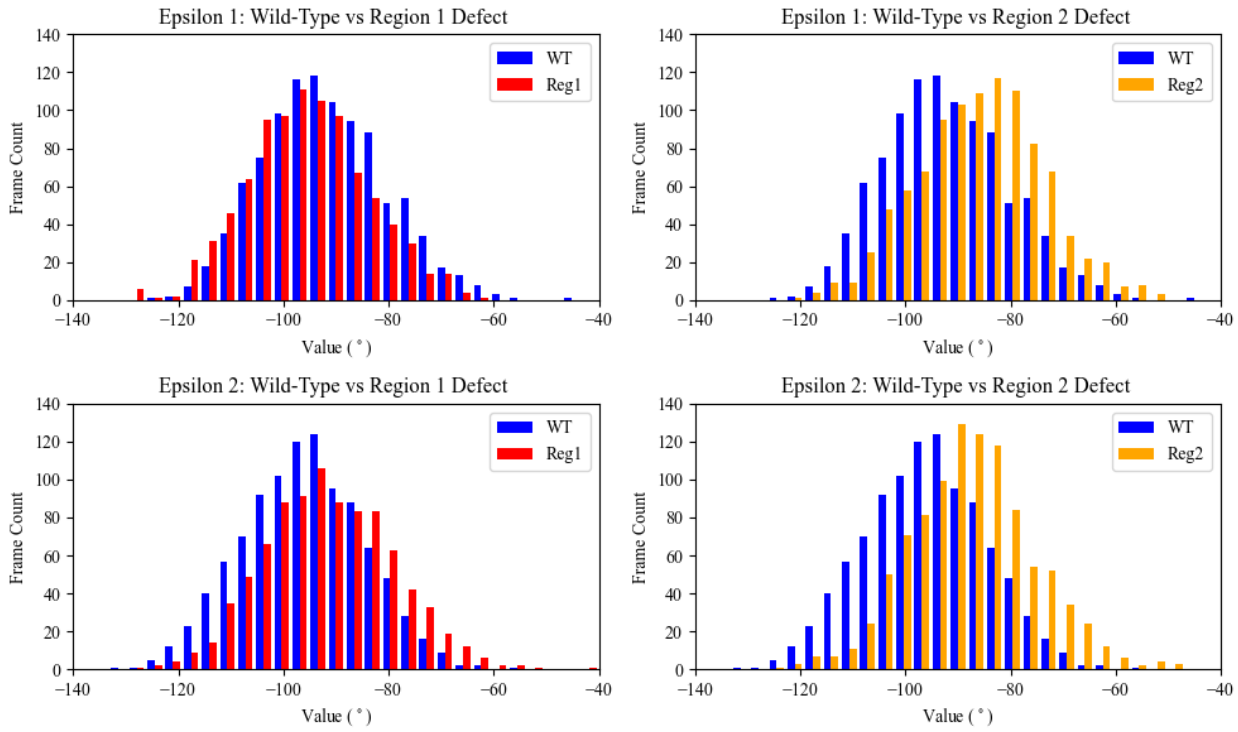

Figure 15: Population distributions of the epsilon torsional angle of both DNA strands 1 and 2 for wild-type system (WT, blue) vs region 1 defect system (Reg1, red) and for wild-type system (WT, blue) vs region 2 defect system (Reg2, orange). The systems do not include in their analysis the 40 base pairs associated with tail regions.

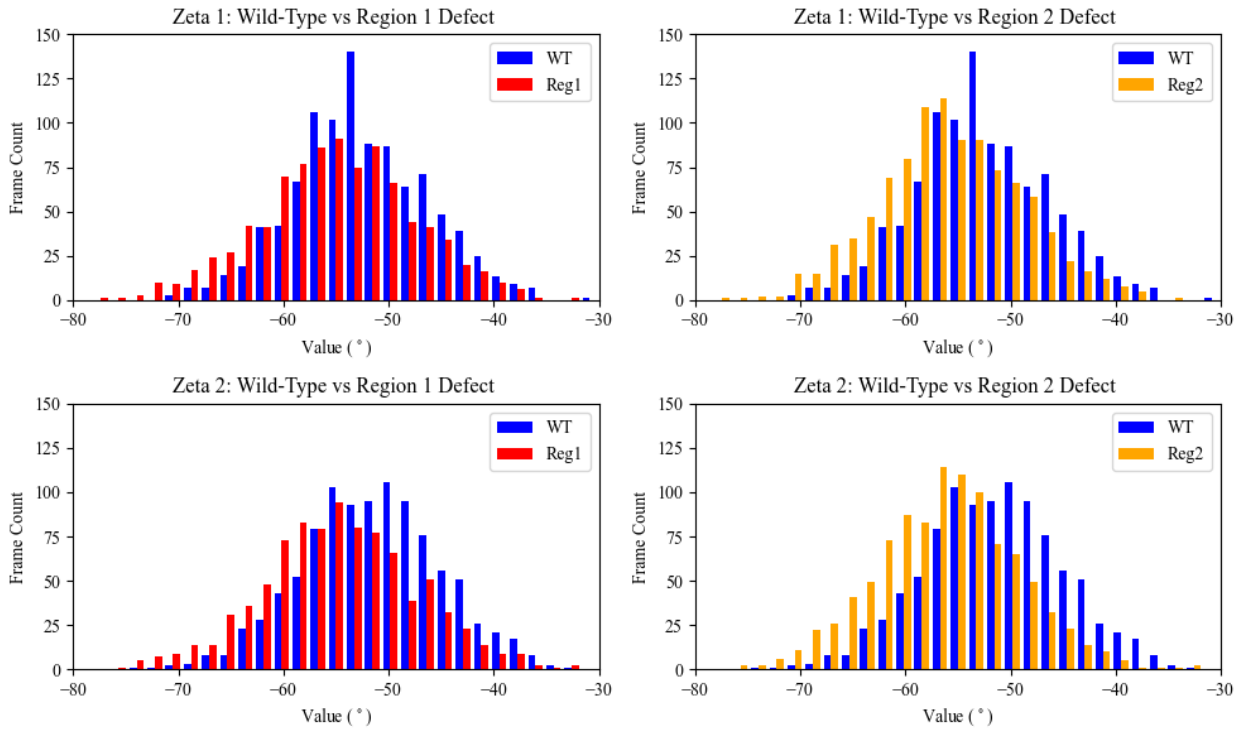

Figure 16: Population distributions of the zeta torsional angle of both DNA strands 1 and 2 for wild-type system (WT, blue) vs region 1 defect system (Reg1, red) and for wild-type system (WT, blue) vs region 2 defect system (Reg2, orange). The systems do not include in their analysis the 40 base pairs associated with tail regions.

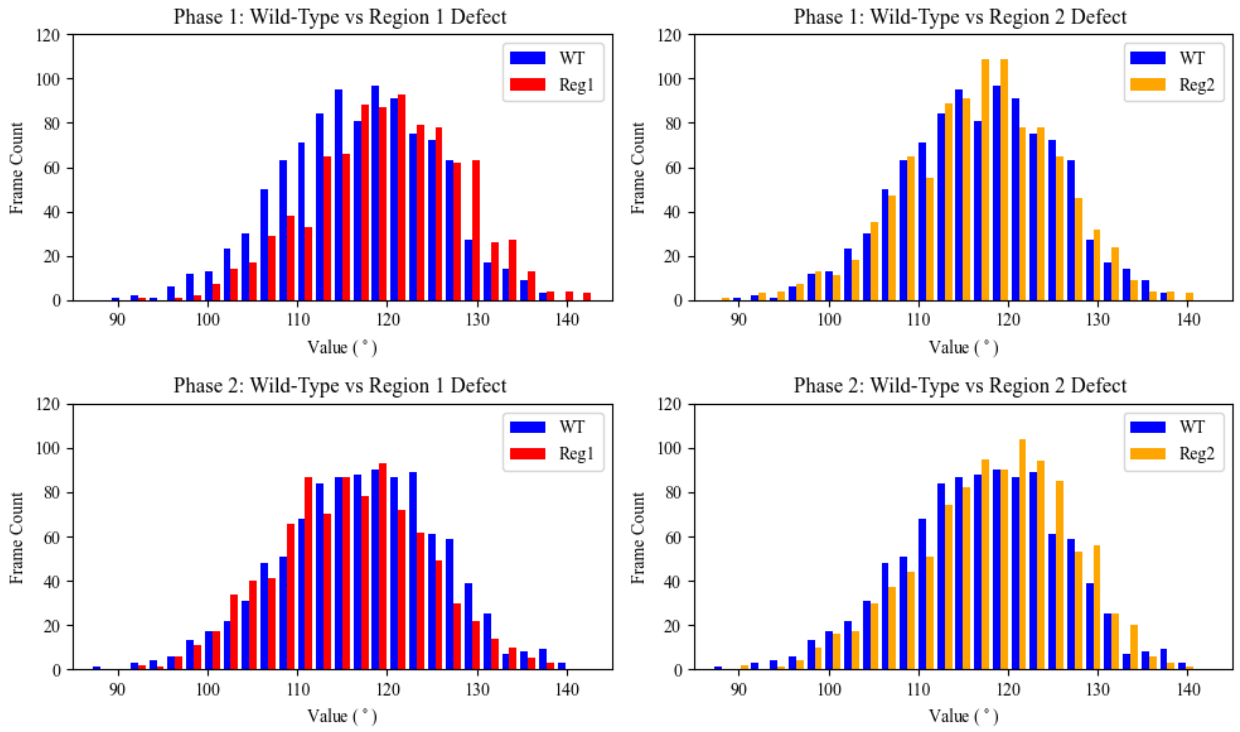

Figure 17: Population distributions of the sugar pucker phase angle of both DNA strands 1 and 2 for wild-type system (WT, blue) vs region 1 defect system (Reg1, red) and for wild-type system (WT, blue) vs region 2 defect system (Reg2, orange). The systems do not include in their analysis the 40 base pairs associated with tail regions.

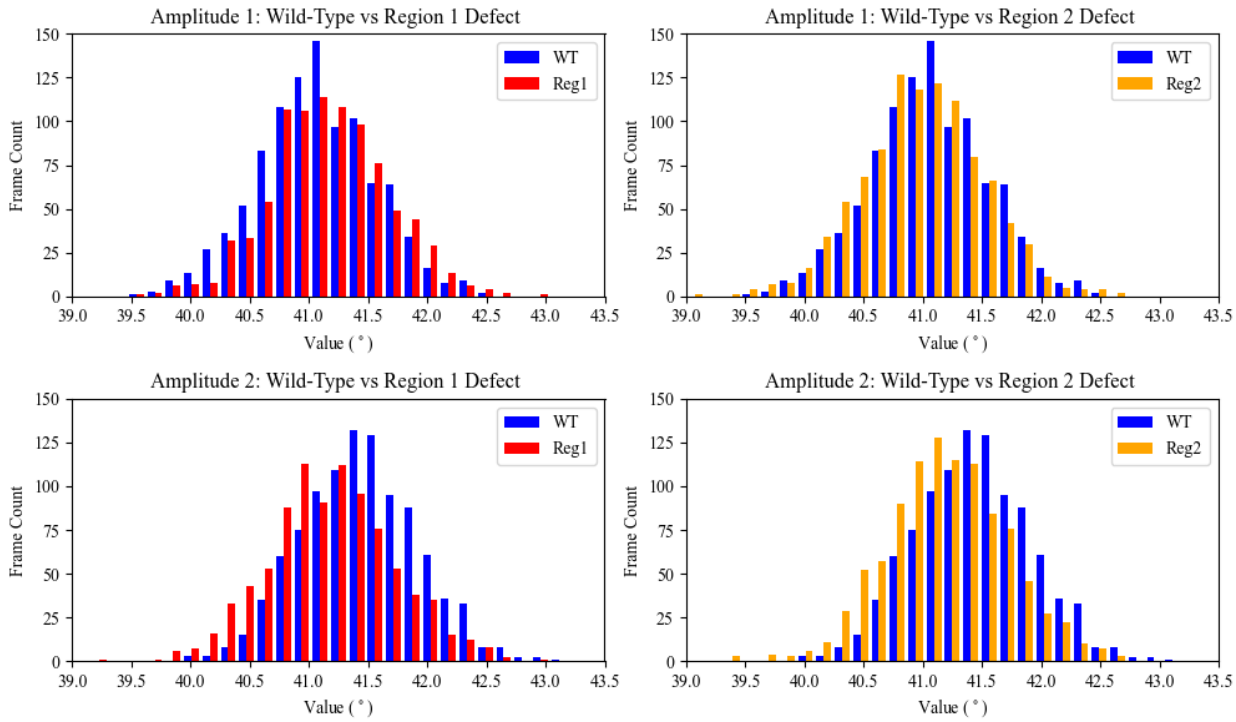

Figure 18: Population distributions of the sugar pucker amplitude of both DNA strands 1 and 2 for wild-type system (WT, blue) vs region 1 defect system (Reg1, red) and for wild-type system (WT, blue) vs region 2 defect system (Reg2, orange). The systems do not include in their analysis the 40 base pairs associated with tail regions.

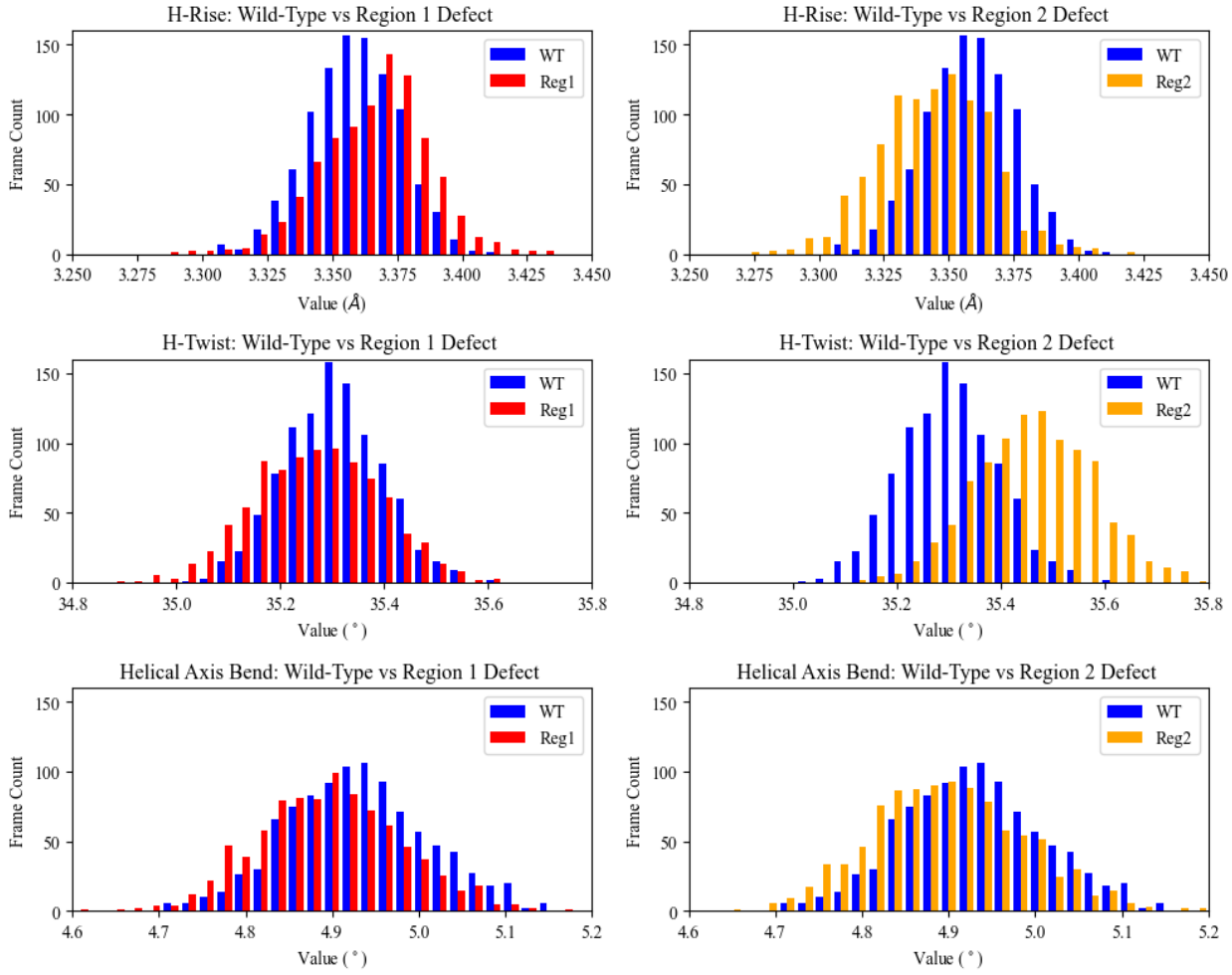

Figure 19: Population distributions of the helical rise, helical twist and the helical axis bend for wild-type system (WT, blue) vs region 1 defect system (Reg1, red) and for wild-type system (WT, blue) vs region 2 defect system (Reg2, orange). The systems do not include in their analysis the 40 base pairs associated with tail regions.

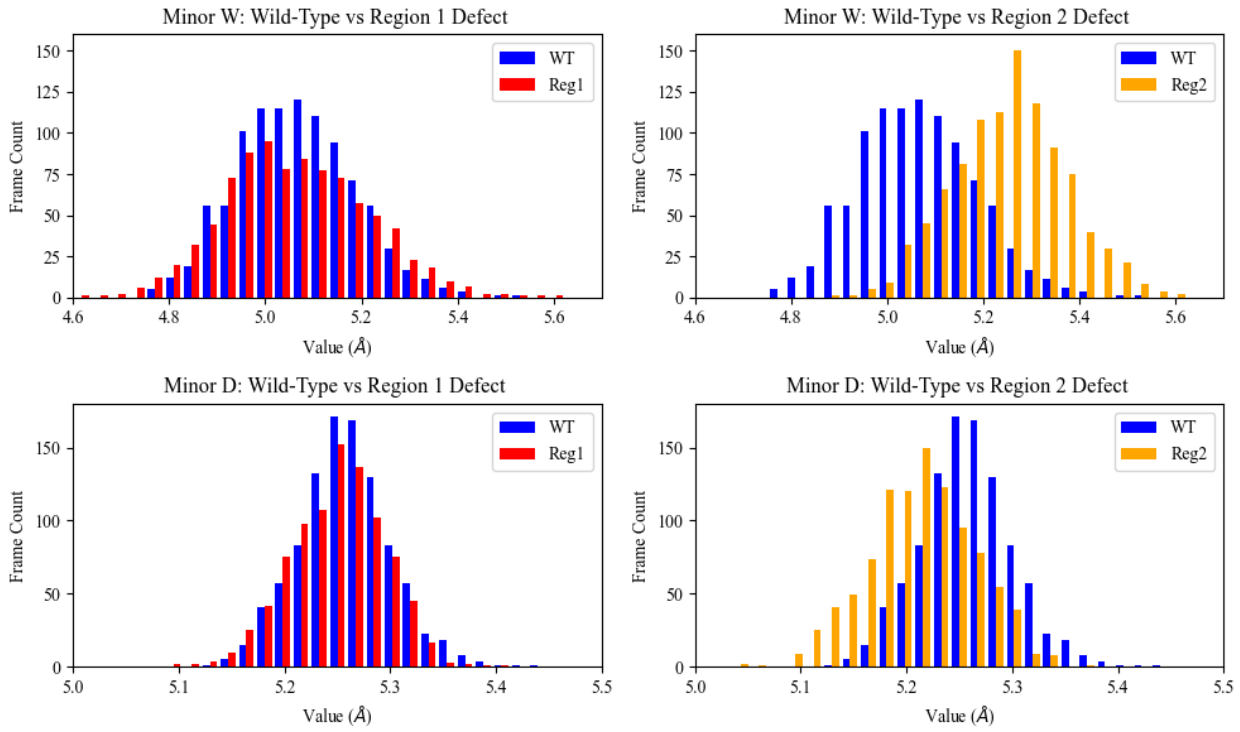

Figure 20: Population distributions of the minor groove width and depth for wild-type system (WT, blue) vs region 1 defect system (Reg1, red) and for wild-type system (WT, blue) vs region 2 defect system (Reg2, orange). The systems do not include in their analysis the 40 base pairs associated with tail regions.

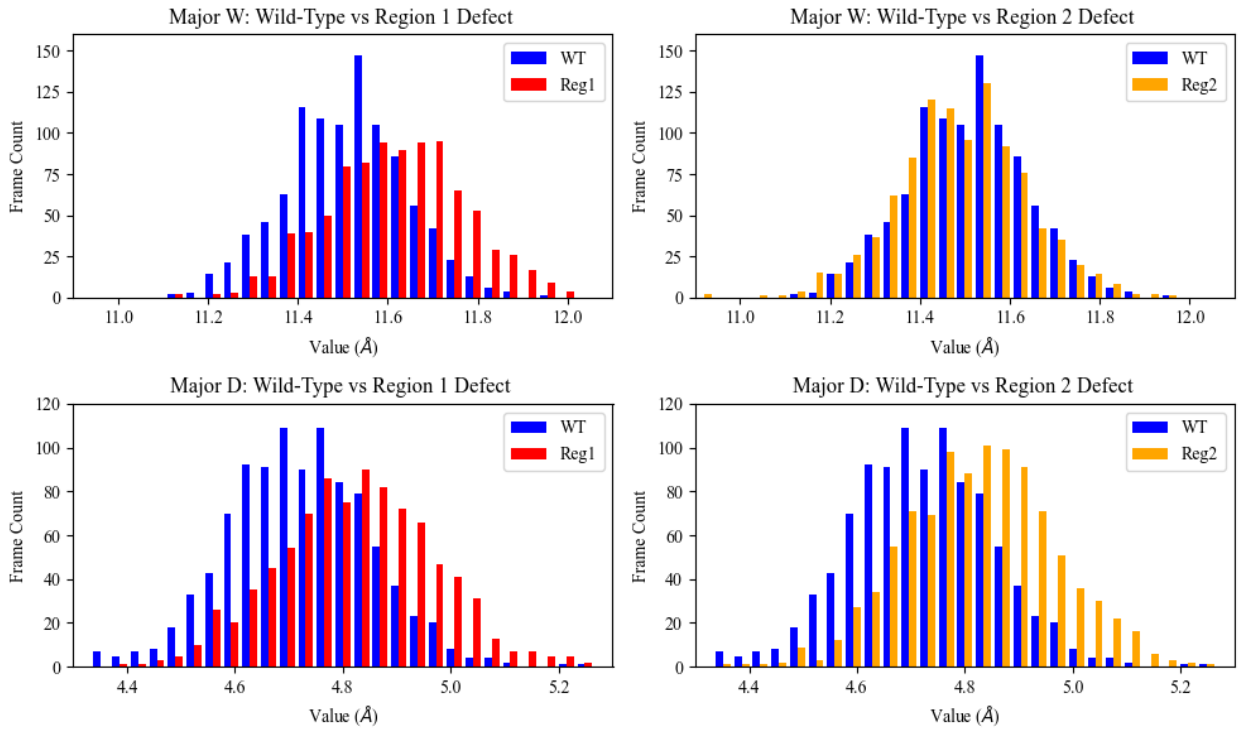

Figure 21: Population distributions of the major groove width and depth for wild-type system (WT, blue) vs region 1 defect system (Reg1, red) and for wild-type system (WT, blue) vs region 2 defect system (Reg2, orange). The systems do not include in their analysis the 40 base pairs associated with tail regions.

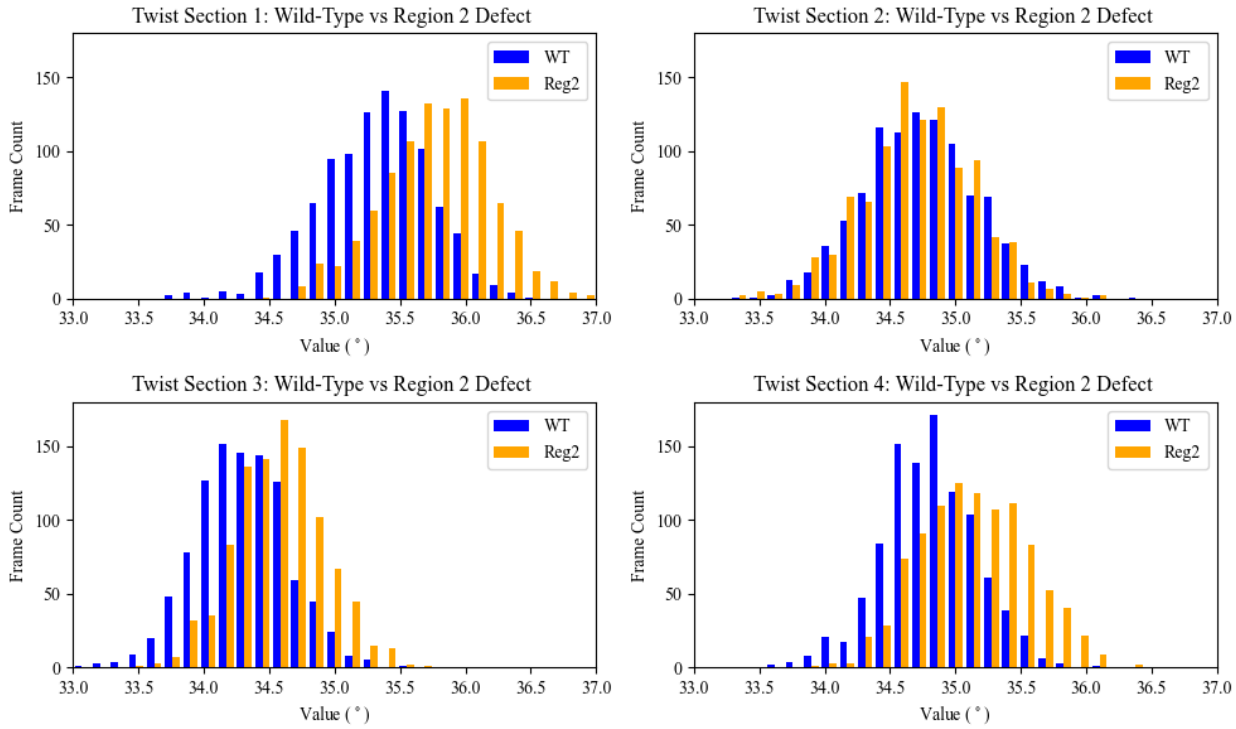

Figure 22: Population distributions of the twist parameter by NCP section for wild-type system (WT, blue) vs region 2 defect system (Reg2, orange).

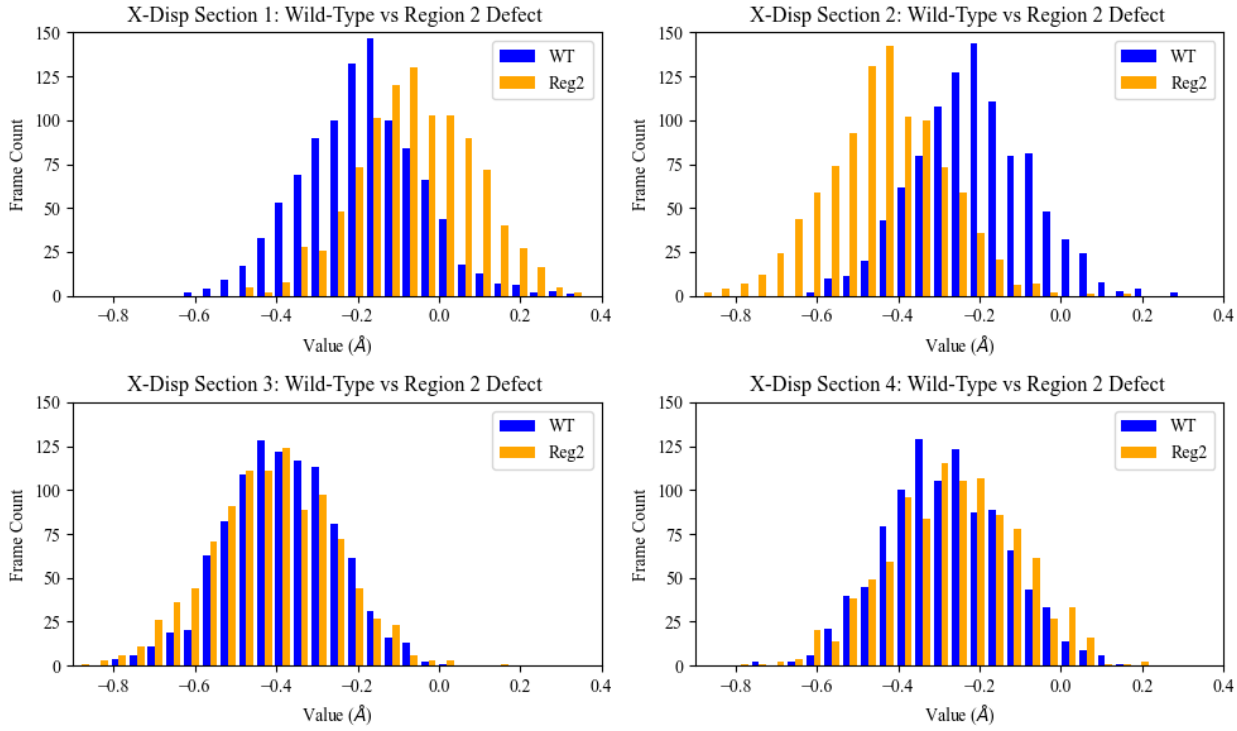

Figure 23: Population distributions of the x-displacement parameter by NCP section for wild-type system (WT, blue) vs region 2 defect system (Reg2, orange).

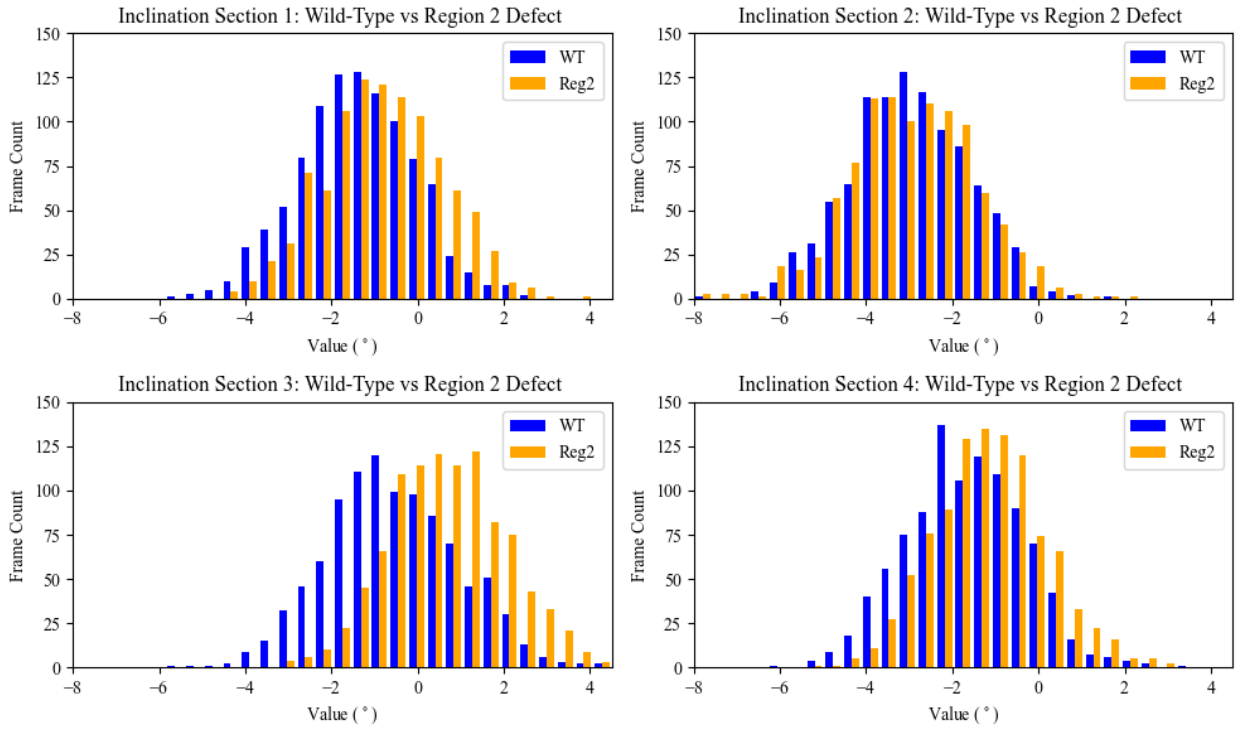

Figure 24: Population distributions of the inclination parameter by NCP section for wild-type system (WT, blue) vs region 2 defect system (Reg2, orange).

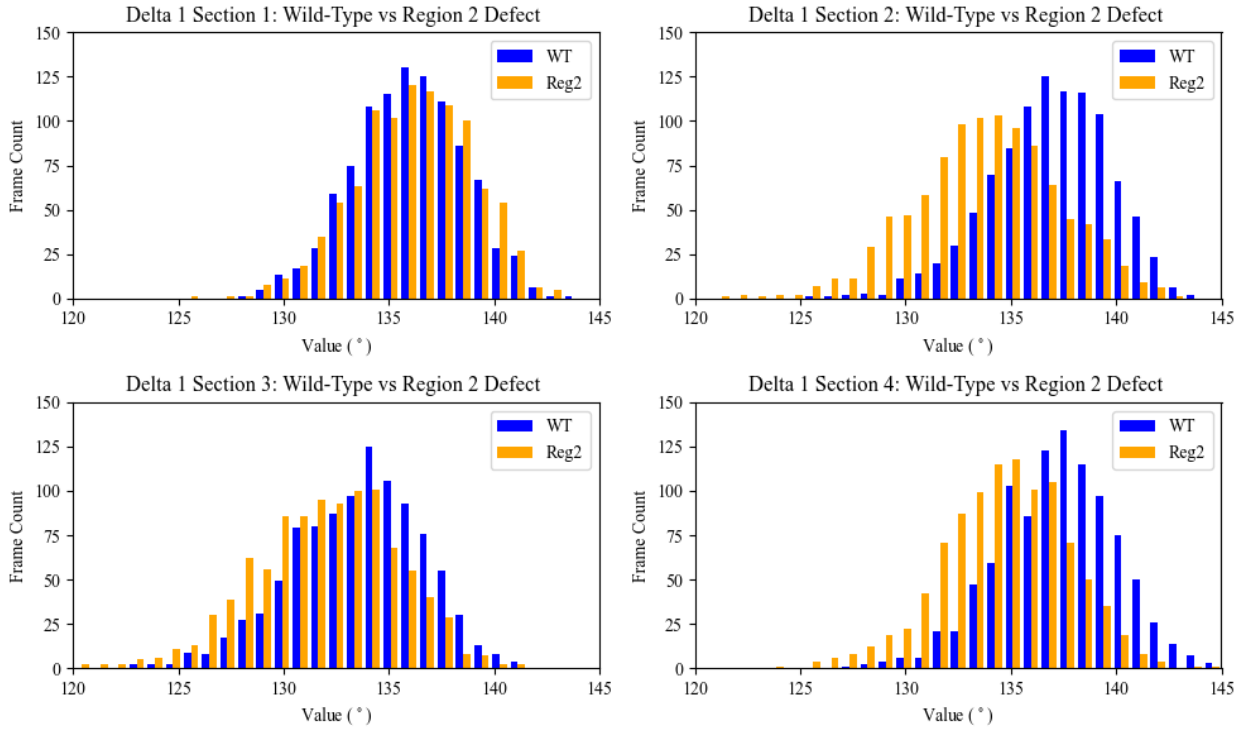

Figure 25: Population distributions of the delta torsional angle on strand 1 by NCP section for wild-type system (WT, blue) vs region 2 defect system (Reg2, orange).

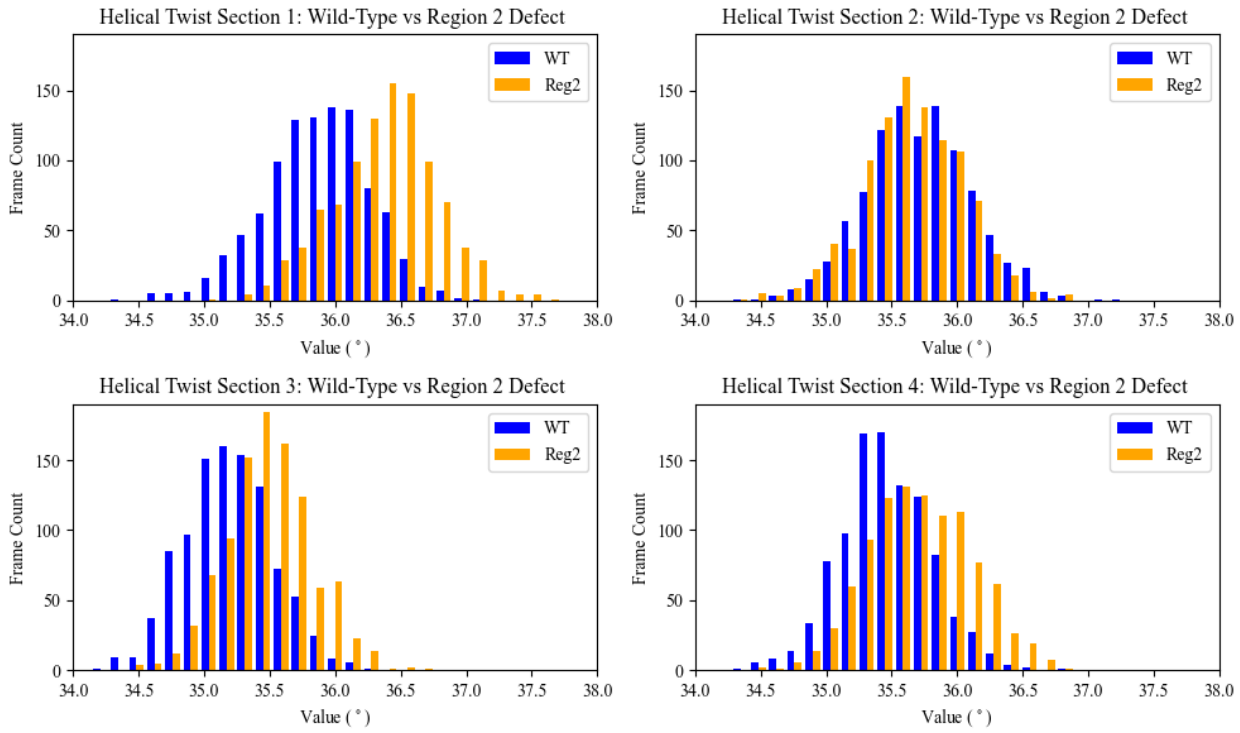

Figure 26: Population distributions of the helical twist parameter by NCP section for wild-type system (WT, blue) vs region 2 defect system (Reg2, orange).

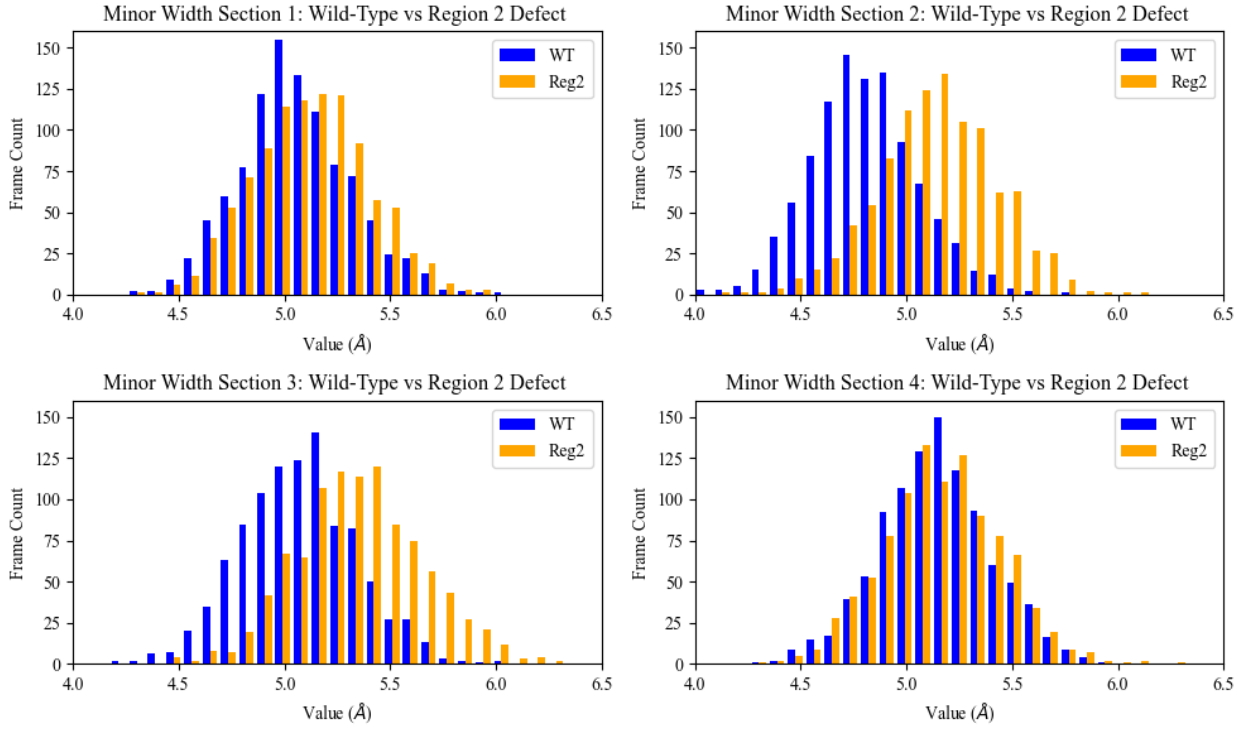

Figure 27: Population distributions of the minor groove width by NCP section for wild-type system (WT, blue) vs region 2 defect system (Reg2, orange).

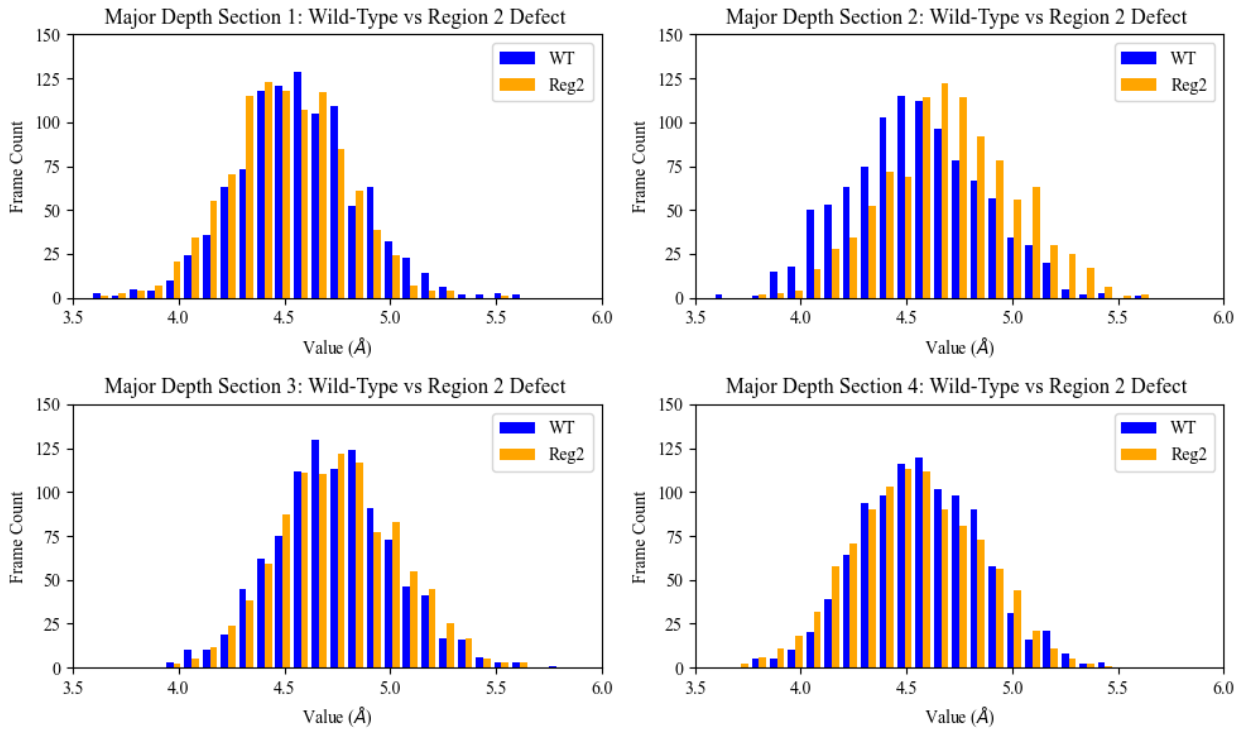

Figure 28: Population distributions of the major groove depth by NCP section for wild-type system (WT, blue) vs region 2 defect system (Reg2, orange).

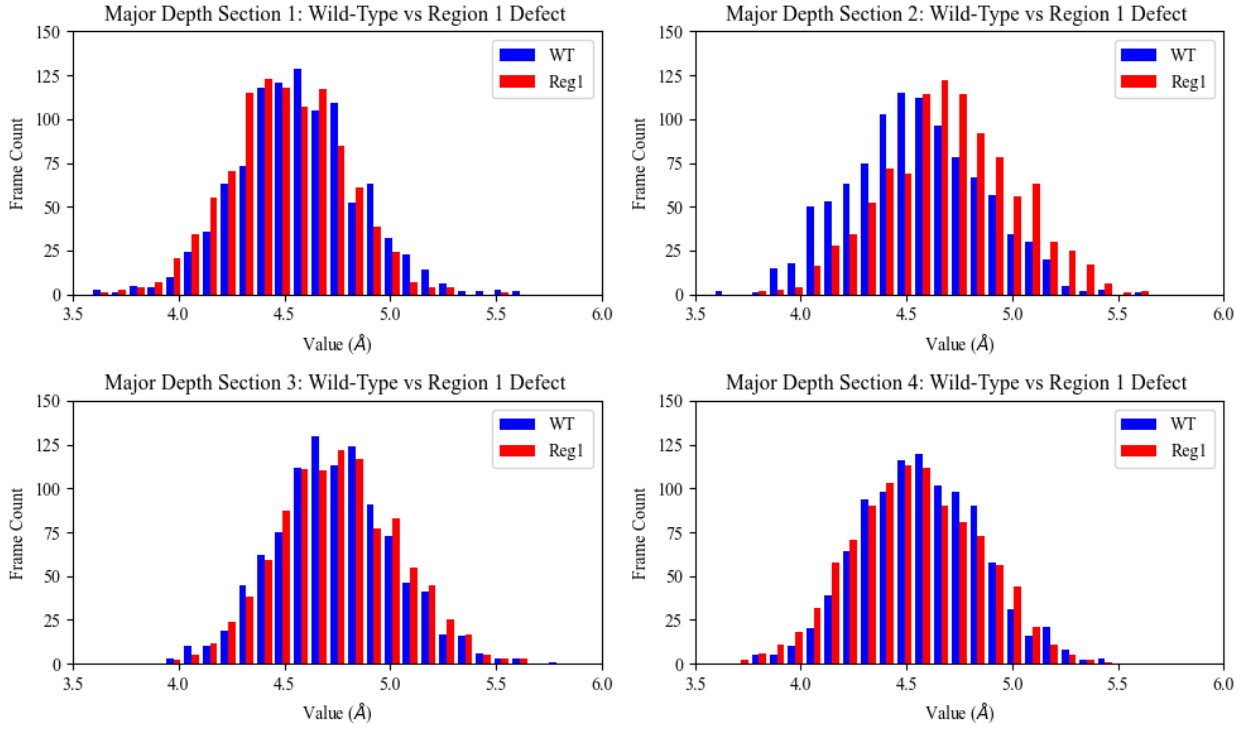

Figure 29: Population distributions of the major groove depth by NCP section for wild-type system (WT, blue) vs region 1 defect system (Reg1, red).

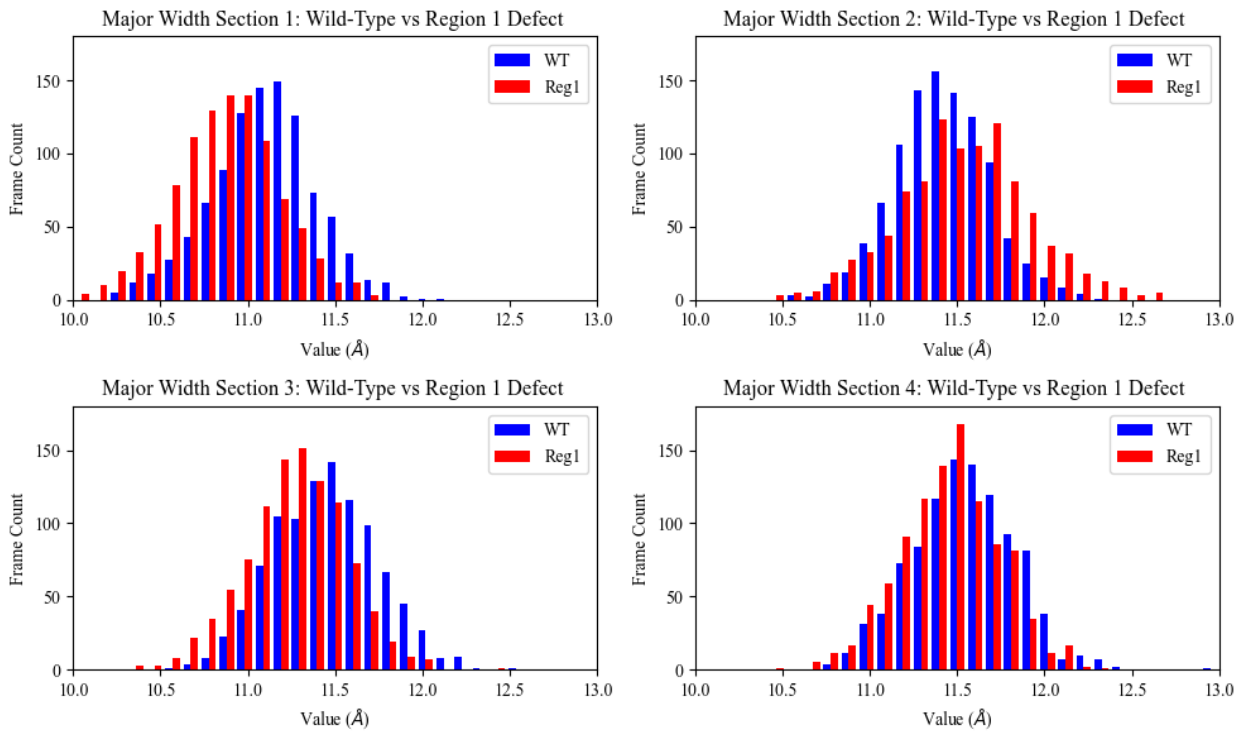

Figure 30: Population distributions of the major groove width by NCP section for wild-type system (WT, blue) vs region 1 defect system (Reg1, red).

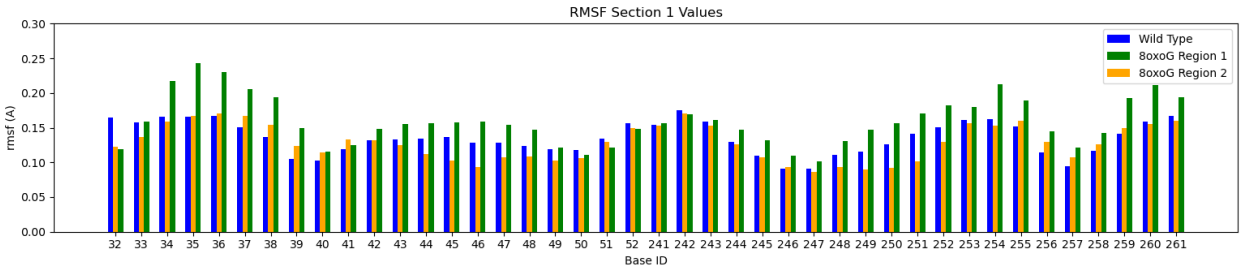

Figure 31: RMSF evaluation of section 1 bases for wild-type system (blue) vs region 1 defect system (green) and vs region 2 defect system (orange).

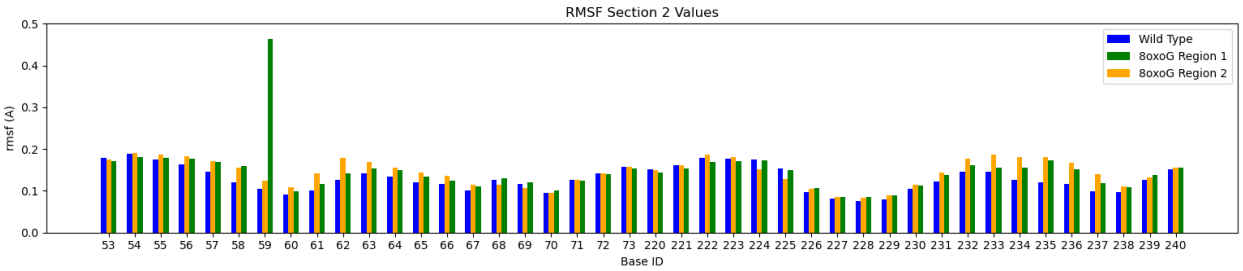

Figure 32: RMSF evaluation of section 2 bases for wild-type system (blue) vs region 1 defect system (green) and vs region 2 defect system (orange).Base number 59 of region 1 is the defect base.

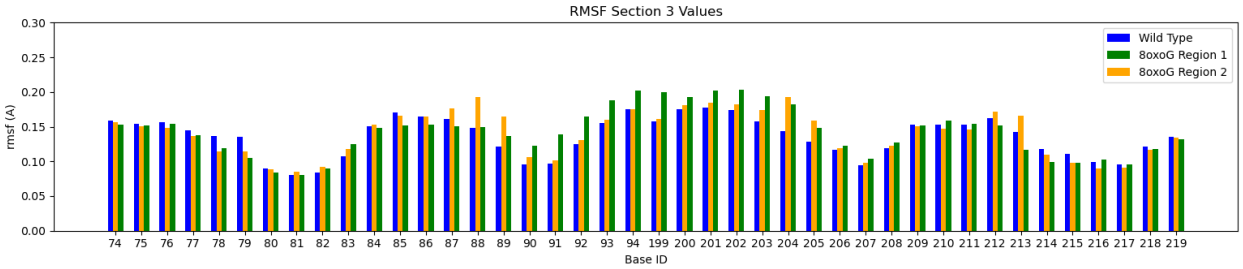

Figure 33: RMSF evaluation of section 2 bases for wild-type system (blue) vs region 1 defect system (green) and vs region 2 defect system (orange).Base number 205 of region 2 is the defect base.

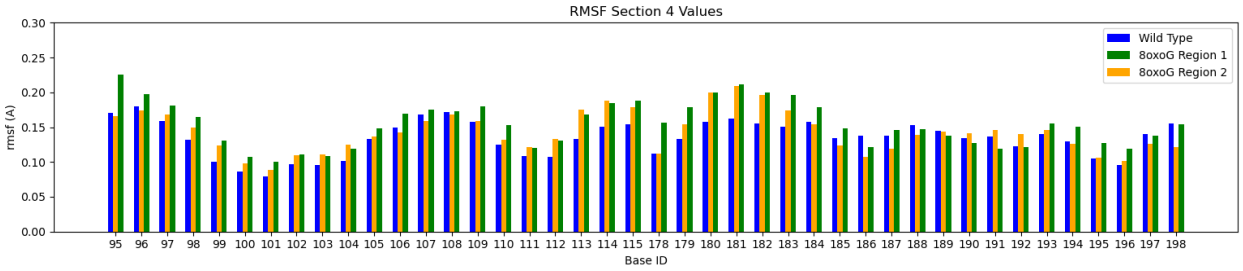

Figure 34: RMSF evaluation of section 3 bases for wild-type system (blue) vs region 1 defect system (green) and vs region 2 defect system (orange).

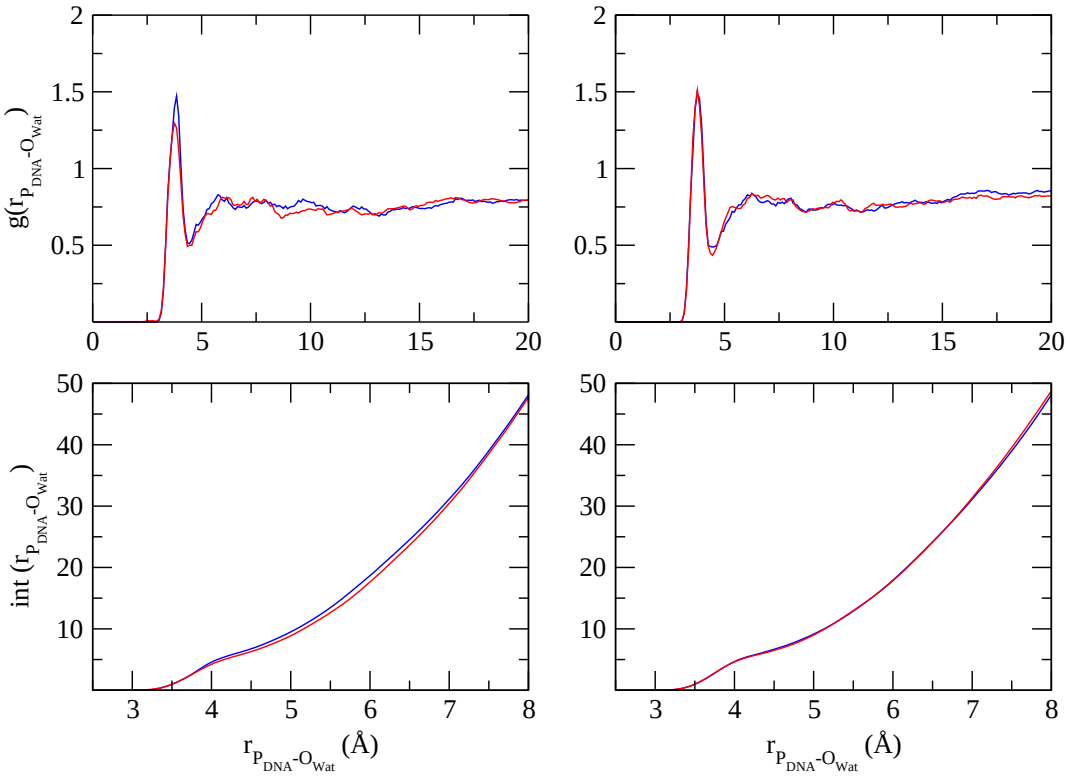

Figure 35: QM DNA-water radial distribution functions g($r_{P-O_{wat}}$), (top) and integrals (bottom) for the P and O_{wat} atoms, for the reduced state (blue colour) and oxidized state (red colour) of the native (left) and defect system (right) of **region 1**.

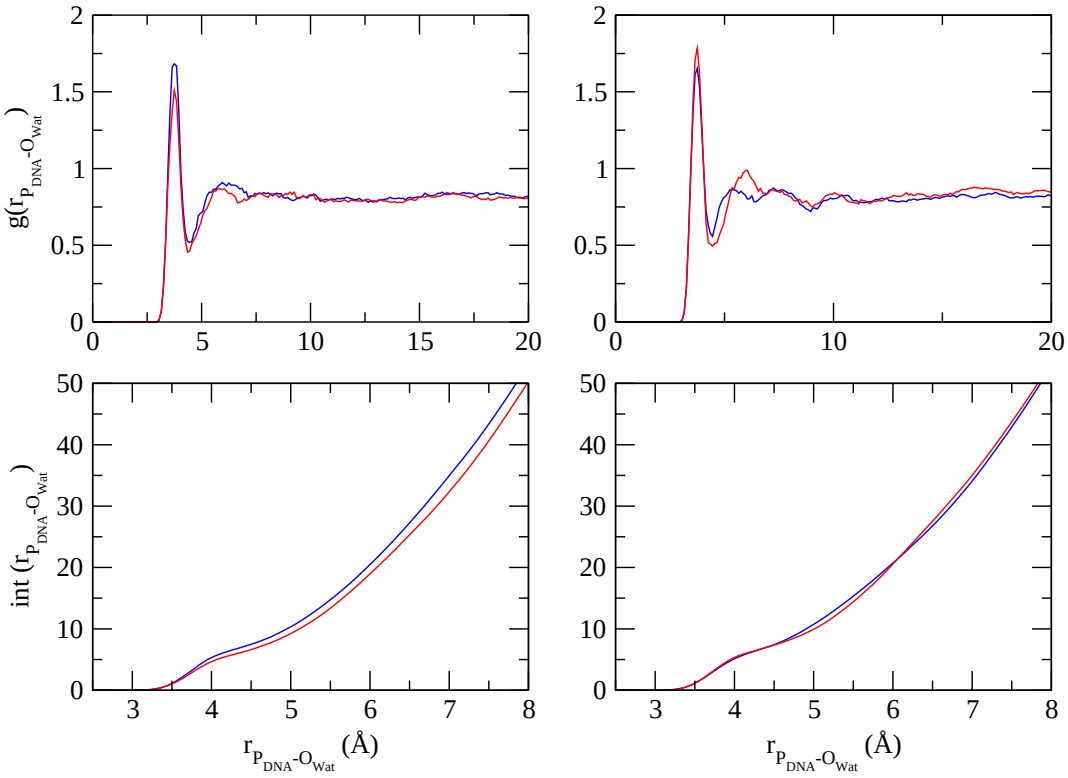

Figure 36: QM DNA-water radial distribution functions g($r_{P-O_{wat}}$), (top) and integrals (bottom) for the P and O_{wat} atoms, for the reduced state (blue colour) and oxidized state (red colour) of the native (left) and defect system (right) of **region 2**.

Author Contributions

† Murat Kılıç and Polydefkis Diamantis contributed equally to the presented work and the preparation of this manuscript.